Pyramidal cell regulation of interneuron survival sculpts cortical networks

Fong Kuan Wong[#1,2], **Kinga Bercsenyi**[#1,2], **Varun Sreenivasan**[1,2], **Adrián Portalés**[1,2], **Marian Fernández-Otero**[1,2], and **Oscar Marín**[1,2]

[1]Centre for Developmental Neurobiology, Institute of Psychiatry, Psychology and Neuroscience, King's College London, London SE1 1UL, United Kingdom

[2]Medical Research Council Centre for Neurodevelopmental Disorders, King's College London, London SE1 1UL, United Kingdom

[#] These authors contributed equally to this work.

Abstract

Complex neuronal circuitries such as those present in the mammalian cerebral cortex have evolved as balanced networks of excitatory and inhibitory neurons. Although the establishment of appropriate numbers for these cells is essential for brain function and behaviour, our understanding of this fundamental process is very fragmentary. Here we show that interneuron cell survival in mice depends on the activity of pyramidal cells during a critical window of postnatal development, in which excitatory synaptic input to individual interneurons predicts their outcome. Pyramidal cells regulate interneuron survival through the negative modulation of PTEN signalling, which effectively drives interneuron cell death during this period. Taken together, our findings indicate that activity-dependent mechanisms dynamically adjust the number of inhibitory cells in nascent local cortical circuits, ultimately establishing the appropriate proportions of excitatory and inhibitory neurons in the cerebral cortex.

In the adult neocortex, approximately one in six neurons are inhibitory gamma-aminobutyric acid-containing (GABAergic) interneurons[1,2], and this ratio is relatively stable across cortical regions and species regardless of total neuronal numbers[3–6]. The cellular balance between excitation and inhibition is critical for brain function and is likely disrupted in a number of neuropsychiatric conditions[7–9]. However, the mechanisms regulating the

establishment of appropriate numbers of excitatory and inhibitory neurons in the cerebral cortex remain largely unknown.

Programmed cell death, also known as apoptosis, is an essential mechanism that sculpts the central and peripheral nervous systems during development[10–12]. The death of developing neurons is mediated by an evolutionarily conserved signalling pathway that involves the pro-apoptotic Bcl2 family members Bax and Bak[13]. Previous studies have shown that both cortical pyramidal cells and GABAergic interneurons undergo extensive cell death during postnatal development[14,15], which suggests that apoptosis may contribute to the establishment of balanced networks of excitatory and inhibitory neurons in the cerebral cortex. However, the temporal relationship and interdependency of the programmed cell death periods for both populations of neurons have not been explored in detail.

Concatenated waves of neuronal death

To determine the developmental sequence that establishes the final ratio of excitatory and inhibitory neurons in the cerebral cortex, we estimated the absolute numbers and relative proportions of pyramidal cells and GABAergic interneurons at different postnatal stages of development using stereological methods in mouse strains in which specific classes of neurons are irreversibly labelled. We chose this method to estimate programmed cell death over the direct quantification of dying cells because classical apoptotic markers such as cleaved caspase-3 have non-apoptotic roles in neurons[16] and are only expressed very transiently (Extended Data Fig. 1a, b). We crossed *Nex*$^{Cre/+}$ and *Nkx2-1-Cre* mice with appropriate reporter strains (see Methods) to identify pyramidal cells and GABAergic interneurons, respectively. Expression of Cre under the control of the *Neurod6* locus in *Nex*$^{Cre/+}$ mice labels all cortical excitatory neurons with the exception of Cajal-Retzius cells[17]. *Nkx2-1-Cre* mice specifically label interneurons derived from the medial ganglionic eminence (MGE) and preoptic area (POA), including the two largest groups of cortical GABAergic interneurons, Parvalbumin (PV+) and Somatostatin (SST+) expressing cells[18].

We observed that the total number of excitatory neurons in the neocortex decreases (~12%) between postnatal day (P) 2 and P5, and then remains stable into adulthood (Fig. 1a, b, e). The reduction in excitatory neurons affects all layers of the neocortex and not only subplate cells (Extended Data Fig. 1c–e), which are known to undergo programmed cell death during this period[19]. By contrast, we found that the number of interneurons is steady until P5, drops extensively between P5 and P10 (~30%), and remains constant into adulthood (Fig. 1c–e). Interneuron cell loss follows the normal maturation sequence of MGE/POA interneurons[20], with deep layer interneurons adjusting their numbers ahead of superficial layer interneurons (Fig. 1f). These results revealed that consecutive waves of programmed cell death adjust the final ratio of excitatory and inhibitory neurons in the developing cerebral cortex.

Interneuron activity predicts cell death

Our results indicated that the adjustment of interneuron numbers is preceded by a wave of pyramidal cell death, which suggest that these two processes might be directly linked. Since

previous work has shown that neuronal activity and apoptosis rates are inversely correlated in the developing brain[21–23], we hypothesised that pyramidal cells may impact interneuron survival by increasing the activity of the cells they connect to. We began testing this idea by monitoring the activity of MGE/POA interneurons in the superficial layers of the barrel cortex (S1BF) during the period of interneuron cell death. To this end, we generated mice expressing the fluorescent reporter tdTomato and the genetically encoded calcium sensor GCaMP6s in MGE/POA interneurons (*Nkx2-1-Cre;RCL^{tdT/GCaMP6s}*)[24] and performed long-term Ca^{2+} imaging in the same interneurons from layer 2/3 S1BF of awake, head-restrained pups (Fig. 2a). To select the most appropriate time for these experiments, we estimated interneuron cell death in S1BF during postnatal development and found comparable dynamics to the rest of the neocortex (Extended Data Fig. 2). For layer 2/3, we observed the most prominent decrease in the number of MGE/POA interneurons between P7 and P8 (Fig. 2b).

We first established our ability to identify surviving interneurons at both times. As expected, we observed that the majority of tdTomato+ interneurons in a region of interest (ROI) were present in the same location the following day (Fig. 2c). However, we also observed that a fraction of tdTomato+ interneurons disappeared between P7 and P8 (Fig. 2c). Since MGE/POA interneurons have ceased migration at the end of the first postnatal week[25], these observations are consistent with the idea that the cells disappearing between P7 and P8 have undergone apoptosis.

We next wondered whether neural activity at P7 in interneurons that die by P8 was different from that of cells that lived past P8. Analysis of calcium event rates (events/min) at P7 indicated that interneurons that died at P8 exhibited significantly fewer calcium events than neurons that lived past P8 (Fig. 2d, e). We next analysed whether P7 event rates could discriminate between neurons that die at P8 and neurons that live beyond this day. Receiver-operating characteristic (ROC) analysis revealed that event rate at P7 performs significantly better than chance in discriminating between these two populations (Fig. 2f). These results suggested that interneurons with relatively low levels of activity immediately before the period of interneuron cell death have an increased probability to undergo apoptosis[26,27].

Pyramidal cells regulate interneuron death

The previous experiments led us to hypothesise that interneurons receiving abundant or particularly strong inputs during the period of interneuron cell death would have increased chances to survive. Since PV+ and SST+ interneurons receive most of their inputs from local pyramidal cells during the first postnatal week[28], we reasoned that modifying the activity of cortical excitatory neurons during the period of interneuron cell death would influence interneuron survival. To test this idea, we transiently modified the activity of pyramidal cells using a chemogenetic approach based on Designer Receptors Exclusively Activated by Designer Drugs (DREADDs) that induce neuronal activation or inhibition[29]. We injected the primary somatosensory cortex (S1) of P0 *Nex^{Cre/+}* (pyramidal cell-specific) mice with the adeno-associated virus (AAV) encoding mutant G protein-coupled receptors that induce neuronal activation (hM3Dq) or inhibition (hM4Di) following administration of the pharmacologically inert molecule clozapine-N-oxide (CNO) (Fig. 3a). We then injected pups

with CNO twice daily between P5 and P8, and examined the distribution of interneurons at P21 (Fig. 3a). We found that increasing the activity of pyramidal cells during the period of interneuron cell death prevents this process and leads to a significant increase in the density of PV+ and SST+ interneurons at P21 compared to control mice (Fig. 3b–d). This effect was not due to activity-dependent changes in the expression of PV or SST or in the density of pyramidal cells (Extended Data Fig. 3a, b). We also found that dampening the activity of pyramidal cells decreases the density of PV+ and SST+ interneurons at P21 compared to controls, which indicates that interneuron cell death can be bi-directionally modulated by modifying the activity of pyramidal cells (Fig. 3b–d). In both types of experiments, changes in the density of interneurons were homogenously distributed across layers containing PV+ and SST+ interneurons (Extended Data Fig. 3c, d). CNO administration did not cause a redistribution of interneurons from neocortical areas adjacent to the injection site (Extended Data Fig. 3e, f). Instead, we observed a prominent increase in the density of cleaved caspase-3 cells following inhibition of the activity of pyramidal cells during the normal period of interneuron cell death (Extended Data Fig. 4a–c). Importantly, control experiments revealed that CNO did not modify the density of PV or SST interneurons in pups not infected with AAV-expressing DREADDs (Extended Data Fig. 4d, e). Similarly, CNO administration between P10 and P13 in hM3Dq- and hM4Di-injected mice revealed no significant changes in the density of PV+ and SST+ interneurons at P21 (Extended Data Fig. 5). Altogether, these experiments demonstrated that pyramidal cells activity is an essential regulator of interneuron survival during the normal period of interneuron cell death.

Interneurons match pyramidal cell numbers

The previous experiments suggest that pyramidal cells 'rescue' appropriate numbers of cortical interneurons from programmed cell death through an activity-dependent mechanism. Based on this idea, we reasoned that modifying the number of pyramidal cells prior to the period of interneuron cell death should also influence the number of surviving interneurons. To test this hypothesis, we generated conditional mice in which pyramidal cells specifically lack *Bak* and *Bax*, whose combined function is critical for apoptosis[30]. As expected, we observed that the number of excitatory neurons in the cerebral cortex of $Nex^{Cre/+};Bak^{-/-};Bax^{fl/fl}$ mutant mice does not decline between P2 and P21 (Extended Data Fig. 6). Consequently, $Nex^{Cre/+};Bak^{-/-};Bax^{fl/fl}$ mutant mice have approximately 12% more pyramidal cells than control animals (Fig. 1b and Extended Data Fig. 6).

We next quantified PV+ and SST+ interneurons in S1 of control and $Nex^{Cre/+};Bak^{-/-};Bax^{fl/fl}$ mutant mice at P21. We found that the density of both PV+ and SST+ interneurons increases by roughly 30% in $Nex^{Cre/+};Bak^{-/-};Bax^{fl/fl}$ mutant mice compared to controls (Fig. 4a, c), which suggests that interneuron cell death is suppressed when pyramidal cell death is prevented. This increase is homogenously distributed across layers containing PV+ and SST + interneurons (Extended Data Fig. 7a), and was also observed in other neocortical areas (Extended Data Fig. 7c, d). To evaluate whether the increase in the number of PV+ and SST + interneurons represents the entire population of cells that should have normally died through programmed cell death, we generated conditional mice lacking *Bax* and *Bak* in MGE/POA interneurons. We found that the density of PV+ and SST+ interneurons also increases by approximately 30% in $Nkx2\text{-}1\text{-}Cre;Bak^{-/-};Bax^{fl/fl}$ mutant mice compared to

controls (Fig. 4b, c). Indeed, fold changes for PV+ and SST+ interneurons were identical for *Nex$^{Cre/+}$;Bak$^{-/-}$;Bax$^{fl/fl}$* and *Nkx2-1-Cre;Bak$^{-/-}$;Bax$^{fl/fl}$* mutant mice (Extended Data Fig. 7b). These results revealed that preventing pyramidal cell death is sufficient to abolish programmed cell death in MGE/POA interneurons, which reinforces the idea that excitatory input from pyramidal cells onto interneurons during early postnatal development is critical for establishing the appropriate ratio of excitatory and inhibitory cells in the cerebral cortex.

PTEN regulates interneuron cell death

We next investigated the molecular mechanisms through which pyramidal cell activity prevents programmed cell death in cortical interneurons. In the developing nervous system, the serine-threonine kinase Akt is a critical mediator of neuronal survival[31,32] that is antagonised by the activity of the phosphatase and tensin homolog PTEN[33,34]. Consistent with this notion, we observed that the relative levels of activated Akt (P-Akt/Akt ratio) transiently increase in the neocortex during the period of interneuron cell death (Fig. 5a). Interestingly, PTEN levels are very heterogeneous among MGE/POA interneurons during the same period (Fig. 5b). PTEN levels are transiently elevated in sparse interneurons in deep and superficial layers of S1 and this increase is concurrent with the peak of interneuron cell death in these layers (Fig. 5c, d and Extended Data Fig. 8a, b). These observations led us to hypothesise that high PTEN levels during this period may drive interneurons towards cell death, and that pyramidal cells might influence this process by regulating PTEN in interneurons.

To test this hypothesis, we generated mice in which we conditionally deleted *Pten* from postmitotic MGE interneurons[35,36]. We observed that *Lhx6-Cre;Pten$^{fl/fl}$* mutant mice have abnormally large jaws and reduced body weight compared to their littermates by P16, probably due to the embryonic expression of *Lhx6* in the first branchial arch[37], which prevented their analysis at later developmental stages. We nevertheless found that *Pten* conditional mutants have a significant increase in the density of PV and SST interneurons in S1 compared to control mice (Fig. 5e, f, g and Extended Data Fig. 8c, d), without changing their relative distribution across layers (Extended Data Fig. 8e). Since *Lhx6-Cre* drives recombination in endothelial cells in addition to MGE interneurons[35], we examined whether a change in the organisation of neocortical blood vessels might contribute to increased survival of interneurons in conditional *Pten* mutants. We found that the density of blood vessels increases in conditional *Pten* mutants compared to controls (Extended Data Fig. 8c, d). However, this change does not affect the density of pyramidal cells (Extended Data Fig. 8c, d), which rules out an indirect effect of blood vessels on interneuron survival through an increase in pyramidal cell density. To discard a direct effect of blood vessels on interneuron survival, we carried out a second series of experiments using acute pharmacological inhibition of PTEN. We injected the PTEN inhibitor bpV(pic) systemically at P7 and P8 in wild type mice and analysed blood vessel density in S1 at P10 (Extended Data Fig. 9b, c). Mice injected with the PTEN inhibitor did not exhibit increased blood vessel coverage (Extended Data Fig. 9b, c). In contrast, transient PTEN inhibition during the period of interneuron cell death increased the density of MGE interneurons compared to control mice (Extended Data Fig. 9a, d, e). Mice injected with the PTEN inhibitor outside the normal window of interneuron programmed cell death showed similar densities of PV and SST

interneurons than controls (Extended Data Fig. 9f–h). These results revealed that PTEN is most likely required cell-autonomously for interneuron apoptosis during the normal period of interneuron cell death.

Finally, we examined whether pyramidal cell activity influences the survival of interneurons by non-cell autonomously regulating the expression of PTEN levels in these cells during the period of interneuron cell death. To this end, we carried out DREADDs experiments similar to those that led to an increased number of cortical interneurons following transient activation of pyramidal cells between P5 and P8 (Fig. 3), but here we analysed PTEN levels in cortical interneurons at P8 (Fig. 5h). We found that PTEN levels are significantly decreased in GABAergic interneurons following the activation of pyramidal cells (Fig. 5i, j). These results strongly suggested that pyramidal cells influence the normal process of interneuron programmed cell death through the activity-dependent inhibition of PTEN, which tips the balance between survival and apoptotic signalling pathways in developing interneurons.

Discussion

Our results suggest that interneuron programmed cell death has evolved as a mechanism responsible for adjusting the final ratio of excitatory and inhibitory neurons in the cerebral cortex, a critical milestone in the assembly of cortical circuits38. Although synaptic mechanisms are known to stabilise excitatory-inhibitory ratios in cortical circuits39–41, this effectively requires that the relative proportions of pyramidal cells and interneurons are within certain parameters42–44. Considering the disproportionate expansion of neocortical areas during human evolution45,46, it is tempting to speculate that the dependency of interneuron survival on pyramidal cells provides an evolutionary advantage for the preservation of appropriate ratios of excitatory and inhibitory cells during the rapid increase of pyramidal cell numbers in the primate lineage.

Our work indicates that interneuron cell death is non-cell autonomously regulated by pyramidal cells, which seem to be able to 'rescue' connected interneurons from their intrinsically determined cell death14 by inhibiting the activity of PTEN during a critical window in postnatal development. It is worth noting that a sizable proportion of individuals with autism spectrum disorders (ASD) and macrocephaly carry deleterious mutations in the *PTEN* gene47,48. Our observations indicate that loss of PTEN function is sufficient to disrupt interneuron programmed cell death, which may in turn alter the cellular balance of excitation and inhibition in the cerebral cortex. This mechanism may contribute to deregulation of cortical information processing and social dysfunction in ASD patients carrying PTEN mutations.

The apoptosis rate of pyramidal cells varies among functionally different neocortical areas and even across layers within the same cortical area49. This suggests that the proposed mechanism may sculpt the heterogeneous patterns of interneuron distributions that exist across the cerebral cortex50. Consequently, the regulation of interneuron programmed cell death by pyramidal cells likely contributes to the cytoarchitectonical specialisation of cortical areas.

Methods

Animals

All experiments were performed following the guidelines of King's College London Biological Service Unit and in accordance with the European Community Council Directive of November 24, 1986 (86/609/EEC). Animal work was carried out under licence from the UK Home Office in accordance with the Animals (Scientific Procedures) Act 1986. Both male and female mice were used indiscriminately throughout the study. For stereology on pyramidal cells, $Nex^{Cre/+}$ mice[19] (kindly provided by K.A. Nave) were crossed with $Fucci2$ mice[51] ($RCL^{Fucci2aR/+}$, kindly provided by R.L. Mort). For stereology on MGE/POA interneurons, $Nkx2\text{-}1\text{-}Cre$ mice[20] (JAX008661) were crossed with $RCL^{tdTomato/tdTomato}$ mice[28] (JAX 007909). For $in\ vivo$ calcium imaging experiments, $Nkx2\text{-}1\text{-}Cre;RCL^{tdTomato/tdTomato}$ mice were crossed with $RCL^{GCaMP6s/+}$ mice[29] (JAX024106) to generate $Nkx2\text{-}1\text{-}Cre;RCL^{tdTomato/GCaMP6s}$ mice. All designer receptor exclusively activated by designer drugs (DREADDs) experiments were conducted in mice obtained from crossing $Nex^{Cre/Cre}$ with CD1 mice. To prevent pyramidal cells from undergoing programmed cell death, $Bak^{-/-};Bax^{Fl/Fl}$ mice[33] (JAX006329) were crossed with $Nex^{Cre/Cre}$ mice and the F1 inter-crossed to obtain $Bak^{+/+};Bax^{Fl/Fl}$ and $Nex^{Cre/+};Bak^{-/-};Bax^{Fl/Fl}$ mutants. For MGE interneurons, a similar breeding scheme used $Nkx2\text{-}1\text{-}Cre$ mice instead. For the quantification of pyramidal cells in $Nex^{Cre/+};Bak^{-/-};Bax^{Fl/Fl}$, these mutants were crossed with Fucci2 mice to obtain $Nex^{Cre/+};Bak^{-/-};Bax^{Fl/Fl};RCL^{Fucci2aR/+}$ mutants. $Pten^{Fl/+}$ mice[40] (JAX006440) were crossed with $Lhx6\text{-}Cre$ mice[39] (kindly provided by N. Kessaris) to generate $Lhx6\text{-}Cre;Pten^{Fl/+}$, and F1 inter-crosses led to the production of $Lhx6\text{-}Cre;Pten^{Fl/Fl}$ mutant mice. Mice were obtained from Jackson's laboratories unless otherwise stated.

Histology

Mice were anaesthetised with an overdose of sodium pentobarbital and transcardially perfused with saline followed by 4% paraformaldehyde (PFA). Brains from pups younger than P6 were post-fixed for 4 h while brains from mice older than P6 were post-fixed for 2 h at 4°C. Brains were sectioned either on the sliding microtome at 30 or 40 μm as previously described[52] or on a vibratome at 40 or 60 μm. All primary and secondary antibodies were diluted in PBS containing 0.25% Triton X-100 and 2% BSA. The following antibodies were used: goat anti-CTGF (1:200, Santa Cruz), rabbit anti cleaved-caspase-3 (1:200, Cell Signalling), rabbit anti-dsRed (1:500, Clontech), goat anti-mCherry (1:500, Antibodies-online), rabbit anti-GABA (1:2000, Millipore), mouse anti-GABA (1:500, Sigma), mouse anti-NeuN (1:500, Millipore) mouse anti-parvalbumin (1:1000, Swant), rabbit anti-parvalbumin (1:5000, Swant), rat anti-somatostatin (1:300, Millipore) and rabbit anti-PTEN (1:500, Abcam). We used Alexa Fluor-conjugated secondary antibodies (Invitrogen). For biotin amplification, sections were incubated with biotinylated secondary antibody (1:200, Vector labs), followed by Alexa Fluor-conjugated Streptavidin (1:200, Vector labs). Blood vessels were stained with Isolectin-B4-FITC or Isolectin-B4-Dylight 594 (1:500, Vector labs).

Stereology

The total number of pyramidal neurons and MGE interneurons in the cerebral cortex were estimated using the optical dissector method[53],

$$N = \frac{\sum Q^- \cdot t}{h \cdot asf \cdot ssf}$$

where $\sum Q^-$ is the total number of cells counted, t the mean section thickness, h the height of the optical dissector (17 μm for pyramidal neuron stereology, 18 μm for MGE stereology), adjusting for the guard zones (1 μm) above and below the dissector, asf stands for the area sampling fraction and ssf stands for the section sampling fraction (frequency of sampling). An ApoTome (Zeiss) equipped with a motorised stage and colour camera was connected to a computer with the Stereo Investigator software (MBF Biosciences). The boundaries of the neocortex were first defined with a 2.5x objective (Zeiss).

For pyramidal neurons, sampling was performed with a 63x objective (Zeiss, numerical aperture (NA) 1.4). The counting frame was set at 15 x 15 μm² and the grid size at 400 x 400 μm². The sampling parameters were as follows: asf = 0.0014, ssf = 0.25 (P2); 0.125 (all other ages). For MGE interneurons, sampling was performed with a 40x objective (Zeiss, NA 1.3). For the entire cortex stereology analysis, the counting frame was set at 125 x 125 μm² and the grid size at 900 x 900 μm² (P2), 1200 x 1200 μm² (all other ages). The sampling parameters were as follows: asf = 0.019 (P2); 0.011 (all other ages), ssf = 0.125. For the upper/lower cortical layer stereology analysis, the counting frame was set at 125 x 125 μm² and the grid size at 900 x 900 μm². The sampling parameters were as follows: asf = 0.019, ssf = 0.125. For the stereological analysis of the barrel field, the counting frame was set at 200 x 200 μm² and the grid size at 350 x 350 μm². The sampling parameters were as follows: asf = 0.3265, ssf = 0.125.

In vivo imaging

P6 animals were anesthetized with 2% isoflurane and held in a nose-clamp. Isoflurane concentration during surgery was maintained between 1-2% and the body temperature was maintained at 37°C by a heating pad. The scalp was cleaned with Betadine and cut open to expose the skull covering the dorsal neocortex. The periosteal tissue, surrounding the skull, was gently scraped with a scalpel. The skull was cleaned with Betadine and Ringer's solution. A circular custom-made metal head-post (Luigs and Neumann) was attached over the left-hemisphere with cyanoacrylate glue (Henkel). A thin protective layer of glue was applied over the skull. The glue was allowed to dry for 10 minutes. Dental cement (Paladur) was used to reinforce the attachment of the head-post to the skull. The animal was injected with Buprenorphine (2 μl/g of a 50 μg/ml solution) and returned to its home cage.

At P7, the animal was anesthetized and head-restrained in a custom-made head holder. A 3-mm craniotomy was opened over the posterior-lateral neocortex. This craniotomy encompassed the primary somatosensory cortex (S1). Care was taken not to damage the dura mater. A circular coverslip (3 mm diameter, Harvard Apparatus) was placed over the craniotomy and its edges were sealed with cyano-acrylate glue and reinforced with dental

cement. Following surgery, Dexamethasone (5 μl/g of a 38 μg/ml solution) was injected subcutaneously. The animal was allowed to recover for at least 2 hours in its home cage, following which we commenced imaging at P7.

Imaging sessions lasted for 40-60 min and we imaged the same field of view for consecutive days in 3 mice. TdTomato and GCaMP6s[54] were excited using a Ti-Sapphire laser (Coherent Chameleon) tuned to λ = 930 nm. The emitted photons were collected by two GaAsP detectors through a 20x objective (Olympus, 1.0 NA). The field of view (FOV) measured 385 x 385 μm (512 x 512 pixels). The scan speed was set to 30 Hz and image sequences were obtained in sweeps of 1 minute (1800 images/channel/minute). The average excitation power was between 40 and 50 mW, and this was kept constant over all imaging days.

To correct for motion artefacts, image registration was carried out using custom written spatial cross-correlation methods on the tdTomato channel. Briefly, on every 1 min sweep, a part of the tdTomato image sequence, where the animal was not moving, was chosen and 20 frames were averaged to give a non-moving reference image. Every frame of the tdTomato image sequence was spatially cross-correlated to this reference image and offset along the X- and Y-axes to match the cross-correlation peak. The offsets obtained for each tdTomato frame was applied to the corresponding GCaMP6s frame.

Calcium imaging analysis

Circular ROIs (diameter = 20 pixels) were manually drawn around tdTomato expressing cell bodies. The mean GCaMP6s fluorescence intensity in time was extracted. Changes in fluorescence signal were calculated as F/F_0, where the baseline fluorescence (F_0) is the mode of a kernel density estimate of F (*ksdensity* function in Matlab). Calcium events were detected by setting a threshold of 3% change in fluorescence from baseline.

Receiver-operating characteristic (ROC) curves

To identify whether the calcium event rate (events/min) at P7 could act as a binary classifier in distinguishing cells that will live and cells that die at P8, we plotted the ROC curve[55] by varying the discrimination threshold (which, in this case, is the P7 event rate) and calculated the area under the curve (AUC). To test for statistical significance, the cell labels were randomly shuffled 5000 times. On each shuffle, we calculated the ROC curve and the corresponding AUC. We then compared our observed AUC to the distribution of shuffled AUCs. The p-value is the fraction of shuffled AUCs observed AUC.

Intracranial injections

pAAV8-hSyn-DiO-hM3D(Gq)-mCherry and *pAAV8-hSyn-DiO-hM4D(Gi)-mCherry* were gifts from Bryan Roth (Addgene plasmids #44361 and #44362)[56]. P0 mice were anesthetized with isoflurane and were mounted in a stereotaxic frame. Pups were injected with 600 nl of virus diluted in PBS and coloured with 0.5% Fast Green (Sigma). Injections were targeted for the somatosensory cortex with an injection rate of 10nl/s.

Drugs

For DREADDs experiments, Clozapine-N-Oxide (CNO, Tocris) was dissolved in 5% dimethyl sulfoxide (Sigma) and then diluted with 0.9% saline to either 1 mg/ml or 5 mg/ml. Pups were injected with vehicle (0.05% DMSO) or CNO (1g/10ml) subcutaneously for 4 days, twice daily. For the PTEN inhibitor experiments, dipotassium bisperoxovanadium(pic) dehydrate (bpV(pic), Sigma) was dissolved in 0.9% saline to 0.2 mg/ml. Pups were injected with vehicle (0.9% saline) or bpV(pic) (1g/10ml) intraperitoneally for 2 days, twice daily. All treatments for CNO and PTEN inhibitor experiments were randomly assigned.

Western blotting

Mouse somatosensory cortex tissue was homogenised in RIPA lysis buffer containing 50 mM Tris pH 8, 150 mM NaCl, 2 mM EDTA, 0.5% sodium-deoxycholate, 0.1% SDS, 1% NP-40 and 1X protease inhibitor cocktail (*cOmplete*™ Sigma). Samples were denatured in Laemmli Sample Buffer57 and run on 10% SDS–PAGE gels. Separated proteins were electrophoretically transferred onto PVDF membranes. Membranes were blocked with 5% BSA in TBST (20 mM Tris-HCl pH 7.5, 150 mM NaCl and 0.1% Tween20) for 1 h and probed with rabbit anti-P-Akt (Ser473, Cell Signalling, 1:1000) overnight at 4°C, followed by an HRP-conjugated donkey anti-rabbit antibody (Thermo Fisher, 1:10,000). The blots were developed using ECL femto Western blotting detection reagents and following read-out, they were stripped (Thermo Fisher). After confirming stripping efficiency, an HRP-conjugated mouse anti-Akt antibody (Cell Signalling, 1:1000) was added overnight at 4°C. The blots were developed using ECL western blotting detection reagents the signals were registered and following stripping, an HRP-conjugated rabbit anti-Actin (Sigma, 1:20,000) was added for 1 h at room temperature. Pico ECL Western blotting reagent was used to detect Actin levels. Signals were read on a Li-COR Odyssey Imaging Band intensities were analysed using ImageStudioLite.

Image acquisition

Images used for analysis were obtained from an ApoTome (Zeiss), epifluorescence microscope (Leica), or SP8 confocal microscope (Leica). ApoTome images were taken using the ApoTome function on the Zen2 software. Images obtained with the confocal and epifluorescence microscope were taken using the LAS AF software.

Cell counting

Cortical layers were identified based on their distinct histological characteristics. Layer 1 was identified as a sparsely populated cell layer. The border between layers 2/3 and 4 was distinguished by the higher nuclei density of layer 4. Layer 5 was identified as the layer basal to layer 4 and above layer 6, which contains less densely packed nuclei. Cell density, within cortical layers, was quantified either manually or using custom routines written in Matlab (MathWorks). For manual quantification, all analyses were conducted blind and cells were counted in a rectangular area, 551.5 μm wide at the pia surface within the somatosensory cortex, auditory cortex or motor cortex. Cells were counted without using pseudocolour in Fiji. Automatic quantification was carried out by image segmentation using morphological operations.

To identify PTEN staining intensity in tdTomato+ or GABA+ interneurons, self-designed Cell Profiler58 pipelines were used. Briefly, tdTomato+ or GABA+ interneurons were identified as primary objects using the global Otsu thresholding method and any objects outside the pre-set diameter range (25-100 pixels) were excluded. PTEN intensity was measured under this cell mask.

Blood vessel analysis

The fraction of the total area covered by blood vessels and the average vessel diameter were quantified using "Vessel Analysis", an ImageJ plugin (http://imagej.net/Vessel_Analysis; Govindaraju and Elfarnawany).

Statistical analyses

Unless specified, results were plotted and tested for statistical significance using Prism 7. The samples were tested for normality using the Shapiro-Wilk normality test. Unpaired comparisons were analysed using 2-tailed unpaired Student's *t*-test (normally distributed) and Mann-Whitney test (not normally distributed). Multiple comparisons with single variable were analysed using one-way ANOVA with post hoc Tukey's test (comparing the mean of each column with the mean of every other column) or Dunnett's test (comparing the mean of each column with the mean of a control column) for normally distributed samples. For samples with nonparametric distribution, either Kruskal-Wallis (single measures) or Friedman's test (repeated measures) was performed followed by the post hoc Dunn's test. For multiple comparisons with more than one variable, a two-way ANOVA with post hoc Sidak's test was used. The cumulative distributions of PTEN intensity levels were compared using the Kolmogorov-Smirnov test. Analysis of calcium events rate was carried out in Matlab. In box plots, the central mark indicates the median, and the bottom and top edges of the box indicate the 25th and 75th percentiles, respectively. The whiskers extend to the most extreme data points not considered outliers. Sample sizes were calculated based on similar studies in the literature. All experiments were replicated at least in two different litters.
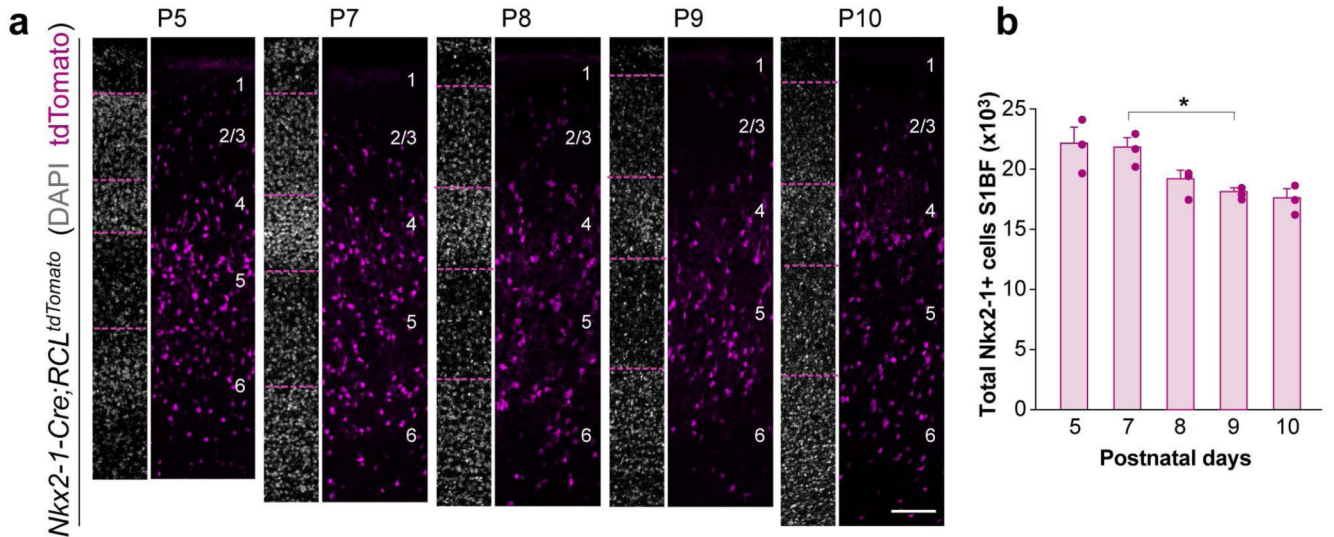
Extended Data
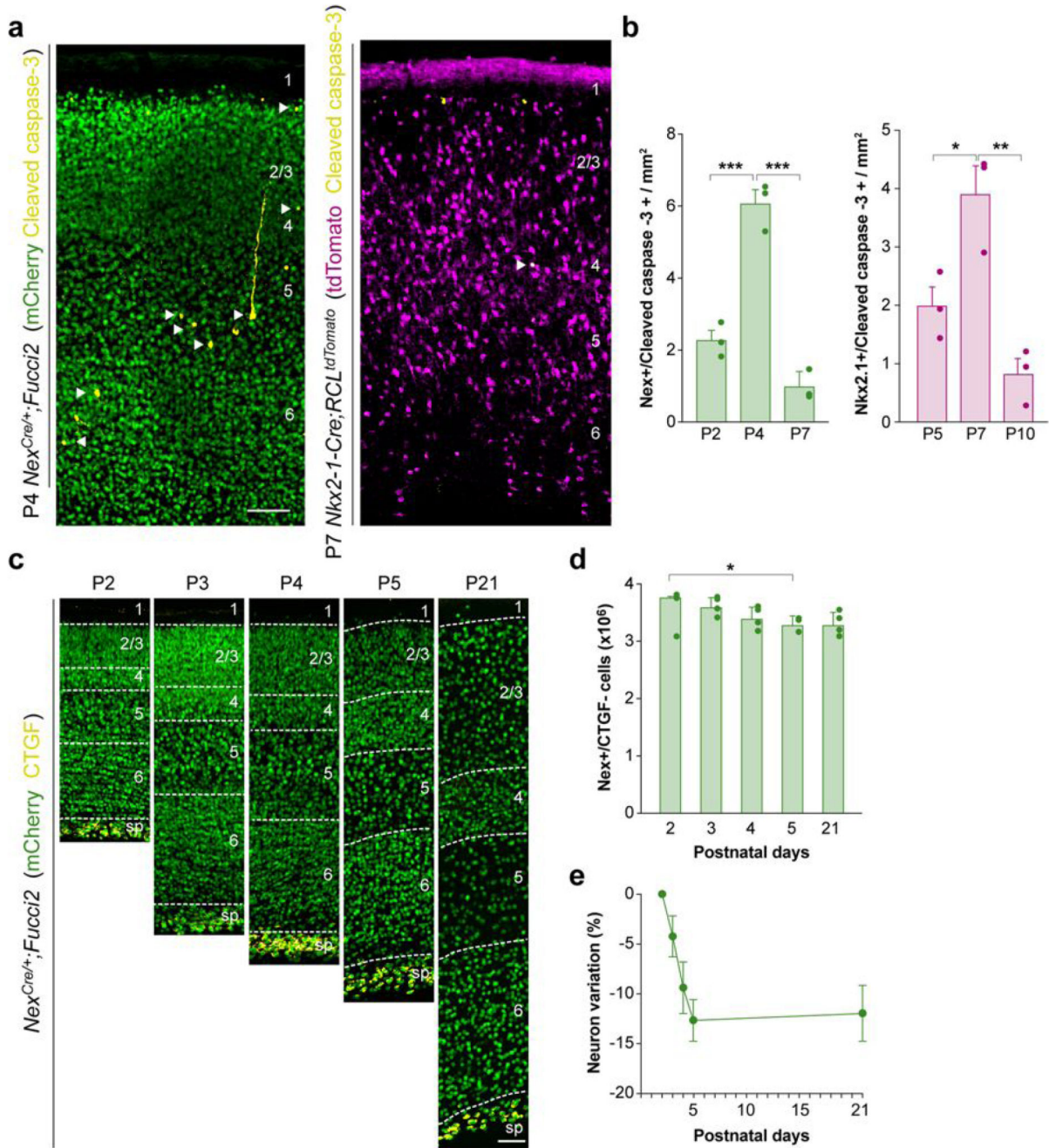
**Extended Data Figure 1. Extensive cell death in layer 2-6 pyramidal cells.**
a, Coronal sections through the S1 cortex of P4 *Nex^{Cre/+};Fucci2* (left) and P7 *Nkx2-1-Cre;RCL^{tdTomato}* (right) mice immunostained for cleaved caspase-3 (yellow) and mCherry (green, left) or tdTomato (magenta, right). **b**, Quantification of density of cleaved caspase-3 cells in pyramidal neurons (left, green bars) and MGE interneurons (right, magenta bars) during postnatal development (for pyramidal neurons, ANOVA, F = 73.6, ***p = 0.003 [P2

vs P4], ***p = 0.00006 [P4 *vs* P7], *n* = 3 animals for all ages; for MGE interneurons, ANOVA, F = 16.91, *p = 0.027 [P5 *vs* P7], **p = 0.0029 [P7 *vs* P10], *n* = 3 animals for all ages). **c**, Coronal sections through the barrel cortex of *Nex^{Cre/+};Fucci2* mice during postnatal development immunostained for mCherry (green) and CTGF (yellow). **d**, Total number of pyramidal cells excluding subplate cells in the neocortex of *Nex^{Cre/+};Fucci2* mice (ANOVA, F = 4.83 and *p = 0.03; *n* = 3 animals for P2 and P5, and 4 animals for P3, P4 and P21). **e**, Temporal variation in the percentage of pyramidal cells excluding the subplate contribution during postnatal development. Data is shown as mean ± SEM. Scale bars, 100 μm.

**Extended Data Figure 2. Interneuron cell loss in the barrel field during postnatal development.**
a, Coronal sections through S1BF of *Nkx2-1-Cre;RCL^{tdTomato}* mice (magenta, MGE interneurons) during postnatal development counterstained with DAPI (grey). **b**, Total number of MGE/POA interneurons in S1BF of *Nkx2-1-Cre;RCL^{tdtomato}* mice during postnatal development (ANOVA, F = 6.40 and *p = 0.03; *n* = 4 animals for all ages). Data is shown as mean ± SEM. Scale bar, 100 μm.
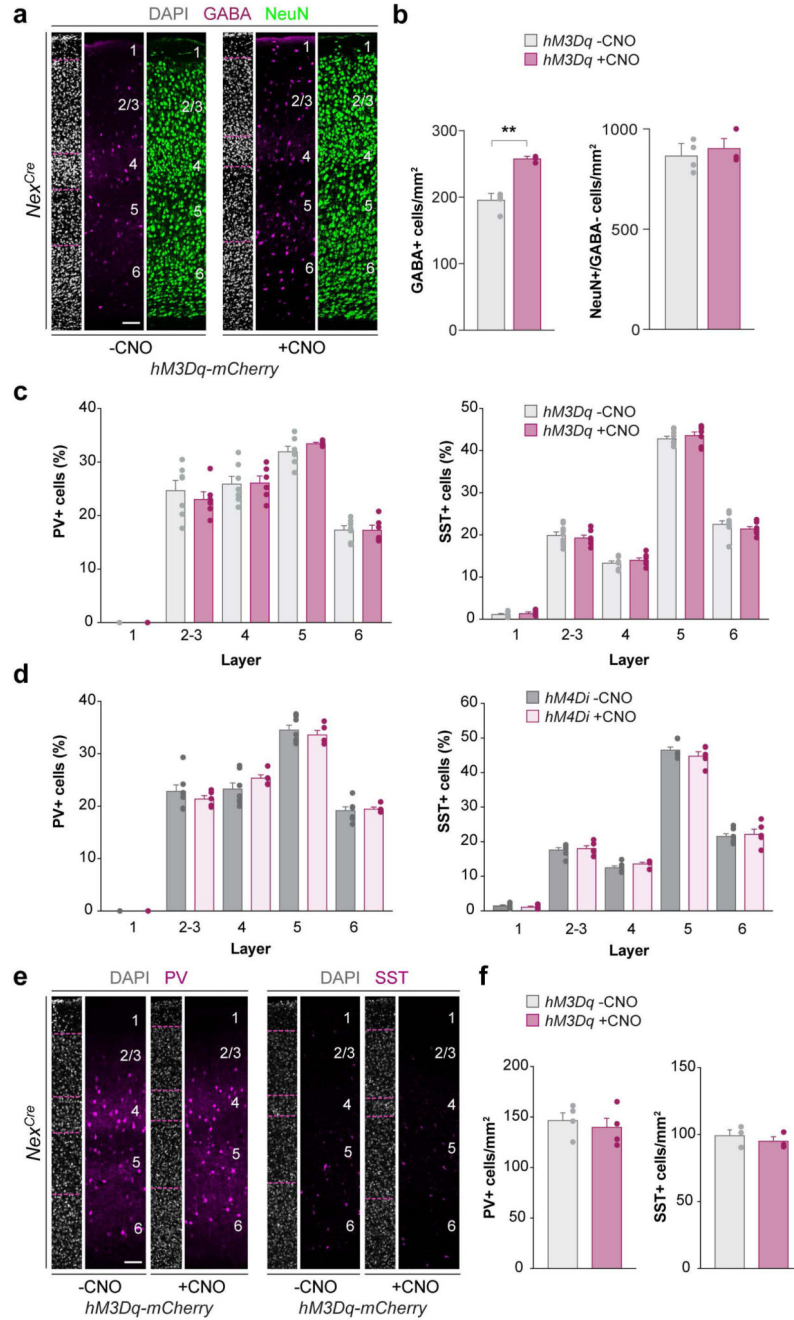
Extended Data Figure 3. Alteration of pyramidal cell activity affects interneuron density but not distribution.

a, Coronal sections through S1BF cortex immunostained for GABA (magenta) and NeuN (green) and counterstained with DAPI (grey) from P21 *Nex^{Cre/+}* mice injected with *hM3Dq-mCherry* virus followed by vehicle or CNO treatment. **b**, Quantification of the density of GABA (left) and NeuN+ but GABA- (right) cells in P21 mice injected with *hM3Dq-mCherry* followed by vehicle (grey bars) or CNO (magenta bars) treatment (2-tailed Student's unpaired *t*-test, **p = 0.005 [GABA], *p* = 0.68 [NeuN+/GABA-], *n* = 4 animals

for vehicle, $n = 3$ animals for CNO conditions). **c, d** Quantification of the distribution of PV (left) and SST (right) in P21 $Nex^{Cre/+}$ mice injected at P0 with *hM3Dq-mCherry* (**c**) or *hM4Di-mCherry* (**d**) and treated with vehicle (grey bars) or CNO (magenta bars) during P5-P8 (2-way ANOVA, $F_{treatment} = 0.48$, $p = 0.50$ [hM3Dq PV], $F_{treatment} = -0.04$, $p = 0.99$ [hM3Dq SST], $F_{treatment} = 0.88$, $p = 0.37$ [hM4DI PV], $F_{treatment} = 0.79$, $p = 0.39$ [hM4DI SST]; for PV, $n = 7$ animals for hM3Dq and hM4DI -CNO, 6 animals for hM3Dq +CNO, and 5 animals for hM4DI +CNO; for SST, $n = 9$ animals for hM3Dq -CNO, 7 animals for hM3Dq +CNO and hM4Di -CNO, and 5 animals for hM4DI +CNO). **e**, Coronal sections through auditory cortex immunostained for parvalbumin (PV, magenta, left) or somatostatin (SST, magenta, right)) and counterstained with DAPI (grey) from P21 $Nex^{Cre/+}$ mice injected with *hM3Dq-mCherry* viruses followed by vehicle or CNO treatment. **f**, Quantification of the density of PV (right) and SST (left) in auditory cortex in P21 mice injected with *hM3Dq-mCherry* followed by vehicle (grey bars) or CNO (magenta bars) treatment (2-tailed Student's unpaired *t*-test, $p = 0.574$ [PV], $p = 0.419$ [SST], $n = 4$ animals for both). Data is shown as mean ± SEM. Scale bars, 100 μm.
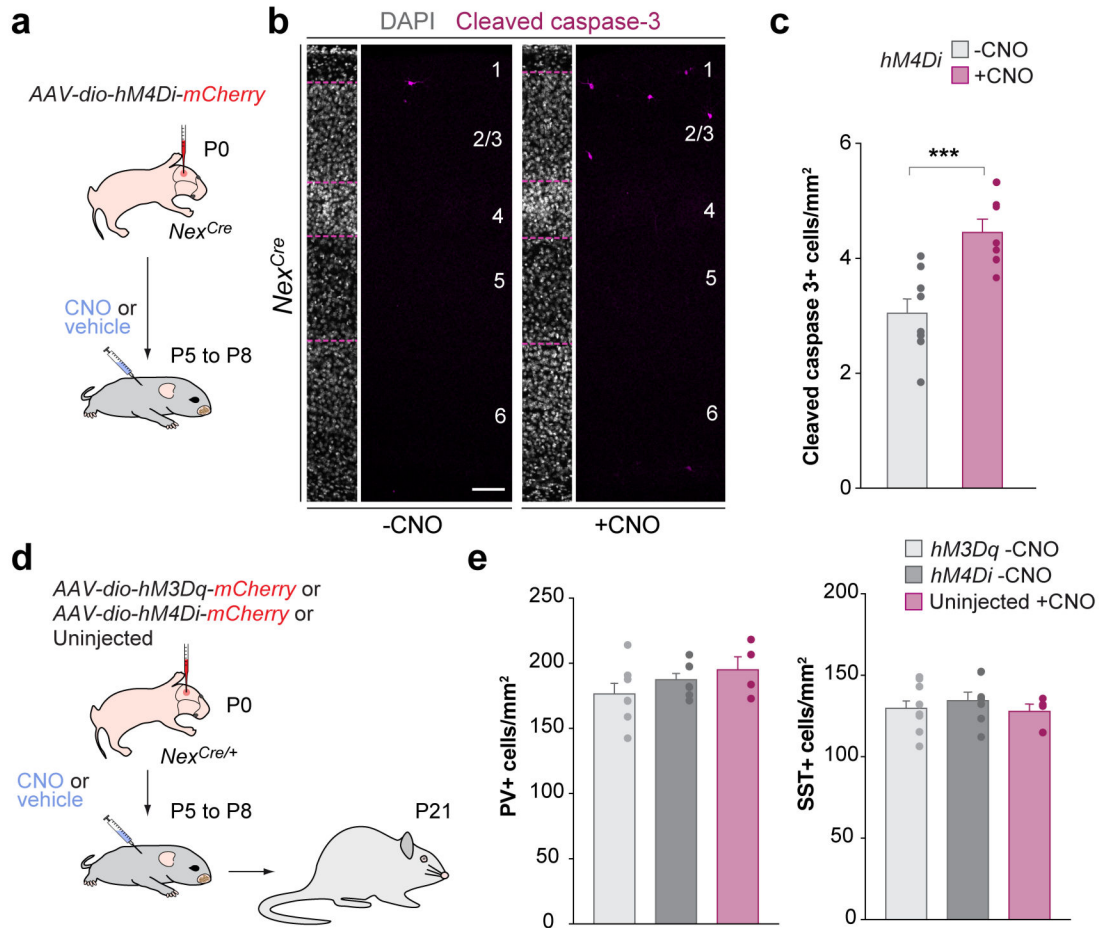
Extended Data Figure 4. CNO control experiments.
a, Schematic of experimental design. **b**, Coronal sections through S1 of P8 *Nex^Cre* mice injected with *AAV8-dio-hM4Di-mCherry* at P0 and treated with (+CNO) or without (-CNO) between P5 and P8, immunostained for cleaved caspase-3 (magenta) and counterstained with DAPI (grey). **c**, Quantification of the density of cleaved caspase-3 cells in P8 mice injected with hM4Di-mCherry and treated (magenta bar) or not treated (grey bar) with CNO between P5-P8 (2-tailed Student's unpaired *t*-test, ***p =0.009, n = 8 animals for -CNO, and n = 7 animals for +CNO). **d**, Schematic of experimental design for CNO control experiments. **e**, Quantification of the density of PV (left) and SST (right) cells in P21 mice injected with *hM3Dq-mCherry* or *hM4Di-mCherry* and not treated with CNO (grey bars), or not injected with viruses and treated with CNO (magenta bars) between P5-P8 (ANOVA, p = 0.24 [PV] and p = 0.65 [SST] for PV, n = 7 animals for hM3Dq and hM4DI -CNO, 4 animals for non-injected +CNO; for SST, n = 9 animals for hM3Dq -CNO, 7 animals for

hM4Di -CNO, and 4 animals for non-injected +CNO). Data is shown as mean ± SEM. Scale bar, 100 μm.
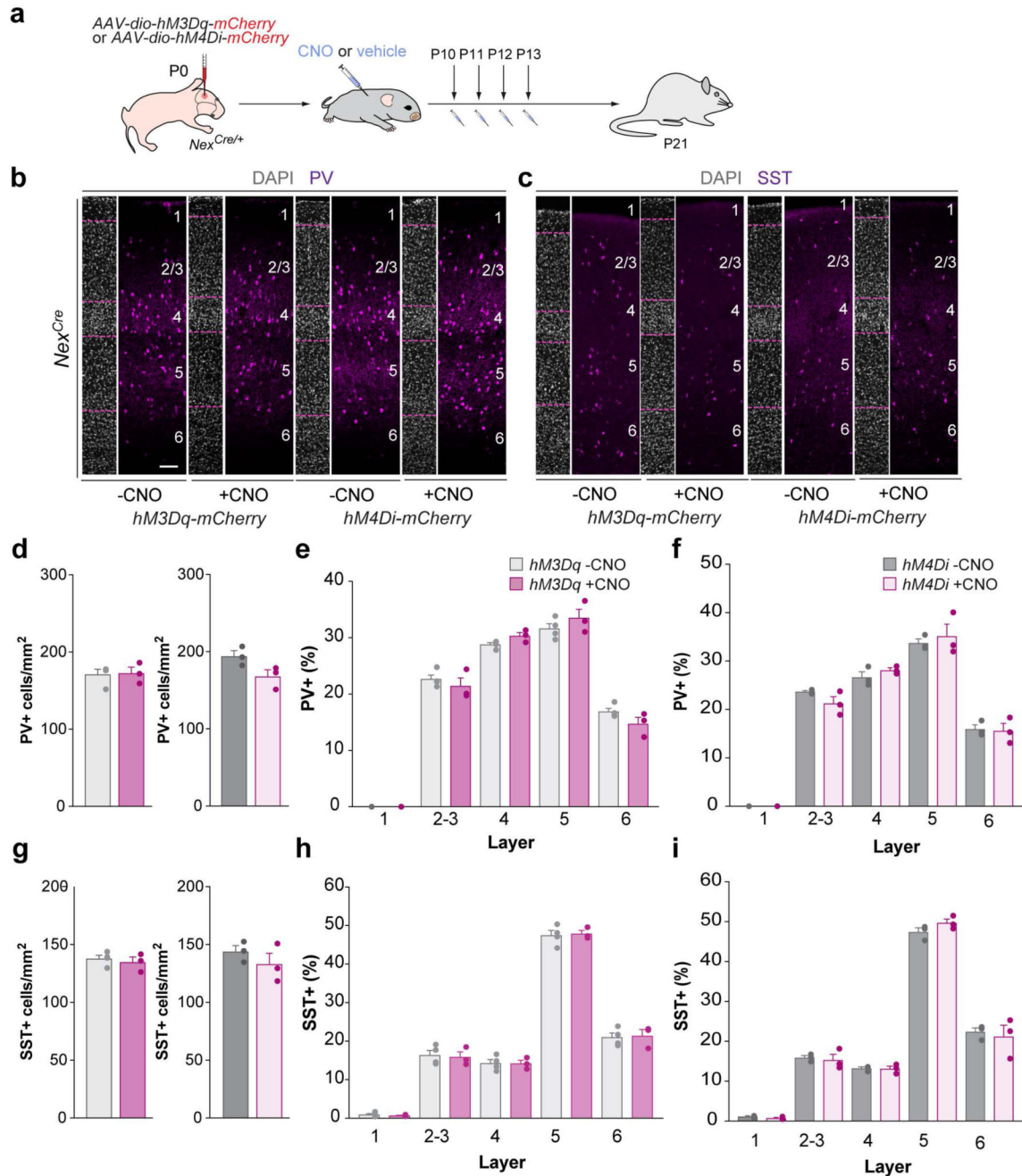
Extended Data Figure 5. Alteration of pyramidal cell activity beyond the normal period of interneuron cell death does not affect interneuron survival or distribution.

a, Schematic of experimental design. **b, c,** Coronal sections through S1BF immunostained for parvalbumin (PV, **b**) or somatostatin (SST, **c**) and counterstained with DAPI (grey) from P21 *Nex^{Cre/+}* mice injected with *hM3Dq-mCherry* (left) and *hM4Di-mCherry* (right) viruses followed by vehicle or CNO treatment. **d, g,** Quantification of the density of PV (**d**) and SST

(**g**) cells in P21 *hM3Dq-mCherry* injected animals (left bars) and *hM4Di-mCherry* injected animals (right bars) followed by vehicle (grey bars) and CNO (magenta bars) treatment at P10-P13 (2-tailed unpaired Student's *t*-test, $p = 0.99$ and $p = 0.087$ respectively; for SST, 2-tailed unpaired Student's *t*-test, $p = 0.56$ and $p = 0.37$ respectively; $n = 4$ animals for hM3Dq –CNO and 3 animals for all other groups)). **e, f, h, i,** Quantification of the distribution of PV (**e, f**) and SST (**h**, **i**) in mice injected with *hM3Dq-mCherry* (**e**, **h**) and *hM4Di-mCherry* (**f**, **i**) followed by vehicle (grey bars) or CNO (magenta bars) treatment at P10-P13 (2-way ANOVA, $F_{treatment} = 0.15$, $p = 0.71$ [hM3Dq PV], $F_{treatment} = 0.60$, $p = 0.48$ [hM3Dq SST], $F_{treatment} = 1.00$, $p = 0.37$ [hM4DI PV], $F_{treatment} = 1.78$, $p = 0.25$ [hM4DI SST]; $n = 4$ animals for hM3Dq –CNO and 3 animals for all other groups). Data is shown as mean ± SEM. Scale bar, 100 μm.
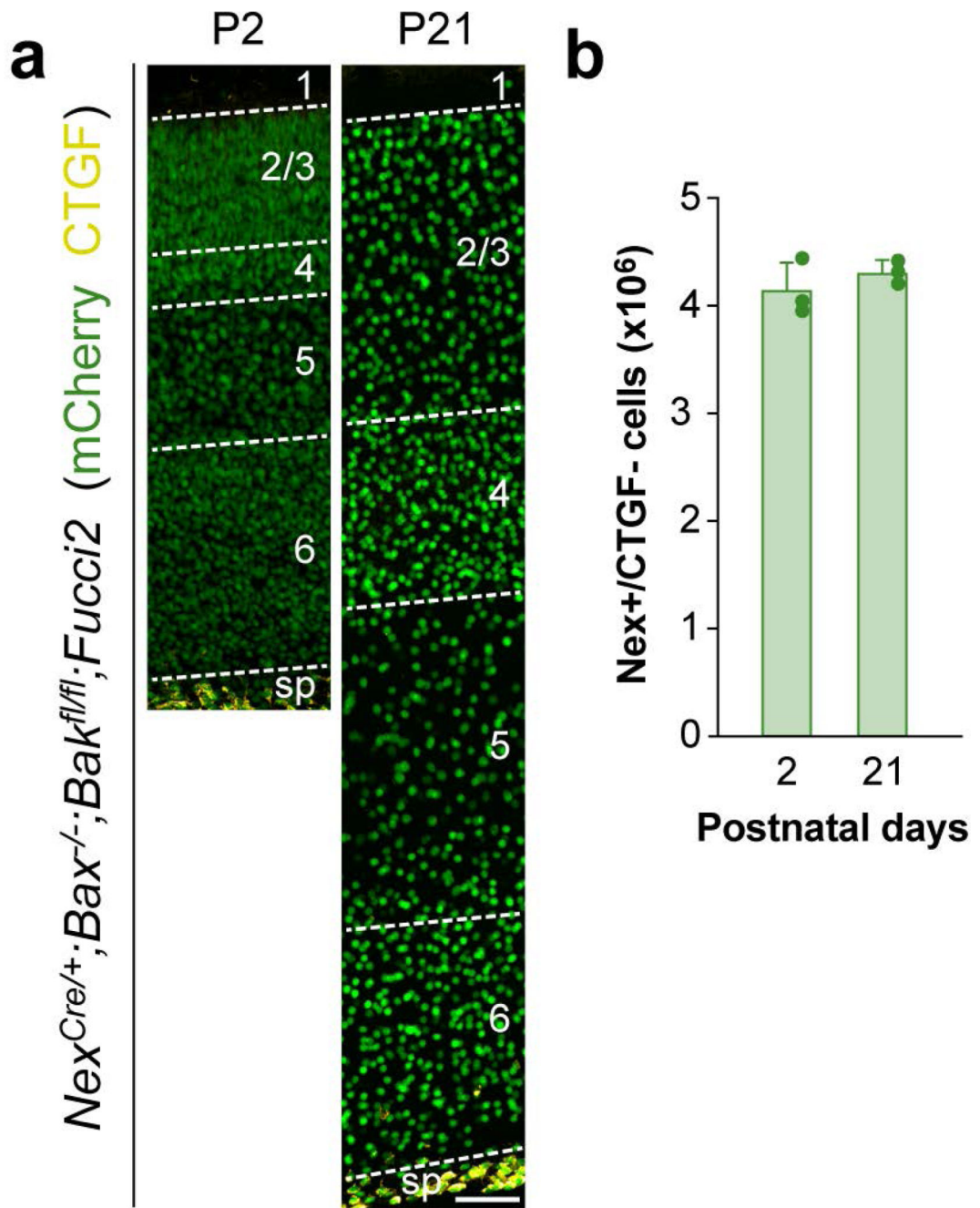
**Extended Data Figure 6. Loss of Bak and Bax prevents programmed cell death in pyramidal cells.**

a, Coronal sections through S1BF from P2 and P21 $Nex^{Cre/+}$;$Bak^{-/-}$;$Bax^{fl/fl}$;$Fucci2$ mice immunostained for mCherry (green) and CTGF (yellow). **b**, Total number of pyramidal cells (excluding subplate cells) in the neocortex of $Nex^{Cre/+}$;$Bak^{-/-}$;$Bax^{fl/fl}$;$Fucci2$ mice (2-tailed Student's unpaired t-test, $p = 0.30$; $n = 3$ animals for both ages). Data is shown as mean ± SEM. Scale bar, 100 μm.
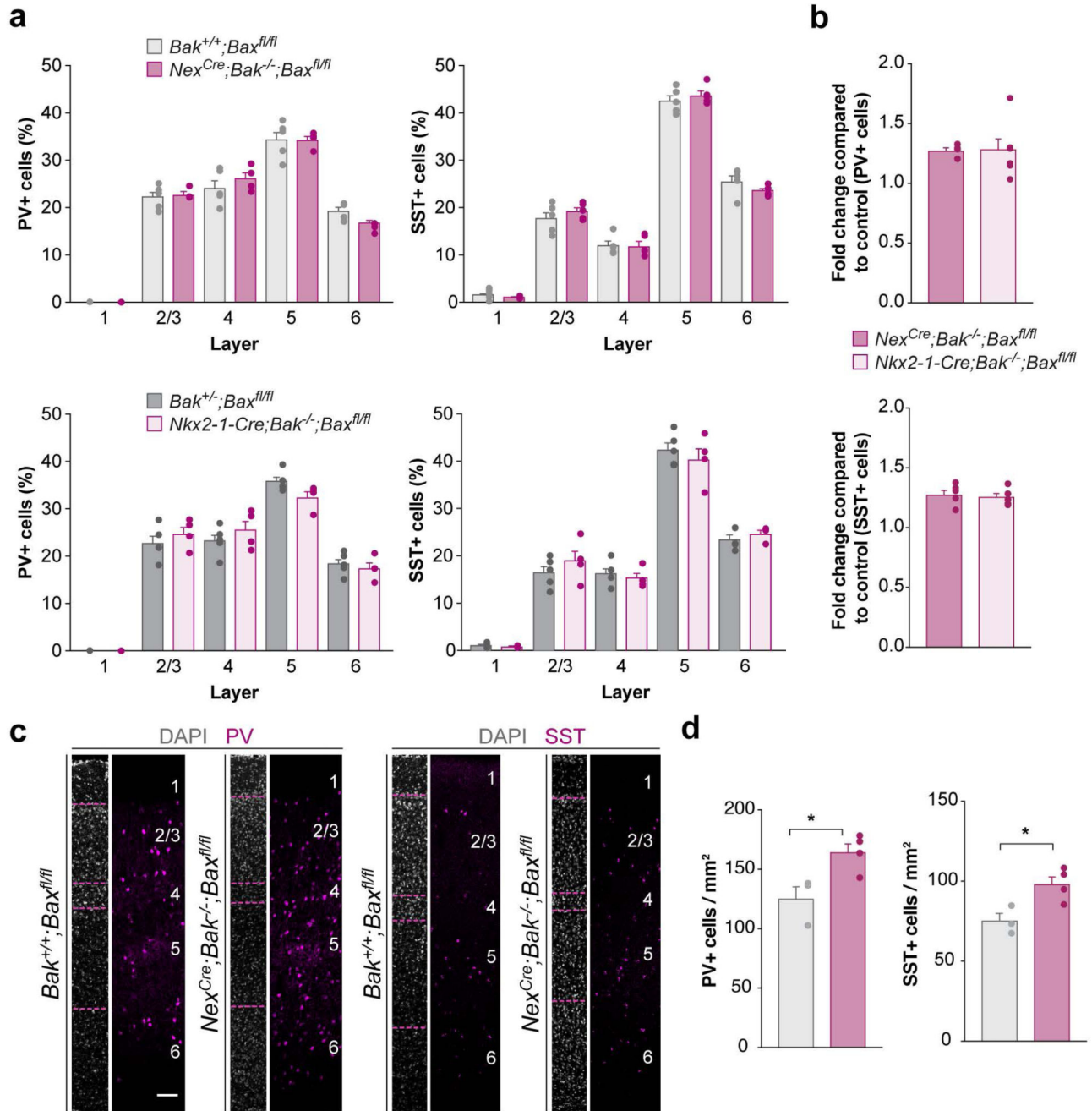
Extended Data Figure 7. Loss of Bak and Bax in pyramidal cells or MGE/POA interneurons affects densities but not lamination of MGE/POA interneurons.

a, Quantification of the distribution of PV (left) and SST (right) interneurons in P30 control (grey bars), $Nex^{Cre/+};Bak^{-/-};Bax^{fl/fl}$ (dark magenta bars) and $Nkx2-1-Cre;Bak^{-/-};Bax^{fl/fl}$ (light magenta bars) mice (2-way ANOVA, $F_{treatment} = 3.56$, $p = 0.10$ [$Nex^{Cre/+}$ PV], $F_{treatment} = 0.44$, $p = 0.53$ [$Nkx2-1-Cre$ PV], $F_{treatment} = 0$, $p = 0.99$ [$Nex^{Cre/+}$ SST], $F_{treatment} = 0.44$, $p = 0.54$ [$Nkx2-1-Cre$ SST], $n = 4$ animals for $Nex^{Cre/+};Bak^{-/-};Bax^{fl/fl}$ [PV] and 5 animals for all other groups). **b**, Quantification of the fold change in the density of PV (top) and SST

(bottom) interneurons in $Nex^{Cre/+};Bak^{-/-};Bax^{fl/fl}$ (dark magenta bars) and $Nkx2$-1-$Cre;Bak^{-/-};Bax^{fl/fl}$ (light magenta bars) mice compared to their respective controls (2-tailed Student's unpaired t-test, $p = 0.90$ [PV], $p = 0.67$ [SST], for PV, $n = 4$ animals for $Nex^{Cre/+};Bak^{-/-};Bax^{fl/fl}$, 6 animals for $Nkx2$-1-$Cre;Bak^{-/-};Bax^{fl/fl}$, for SST, $n = 5$ animals for both $Nex^{Cre/+};Bak^{-/-};Bax^{fl/fl}$ and $Nkx2$-1-$Cre;Bak^{-/-};Bax^{fl/fl}$). **c**, Coronal sections through the motor cortex of P30 $Bak^{+/+};Bax^{fl/fl}$ and $Nex^{Cre/+};Bak^{-/-};Bax^{fl/fl}$ mice immunostained for parvalbumin (PV, left) and somatostatin (SST, right) and counterstained with DAPI (grey). **d**, Quantification of the density of PV (left) and SST (right) cells in the motor cortex control and pyramidal cell-specific Bax/Bak double mutant mice at P30 (2-tailed Student's unpaired t-test, *$p = 0.02$ [PV], *$p = 0.01$ [SST], for PV, $n = 4$ animals for both and for SST, $n = 3$ animals for both). Data is shown as mean ± SEM. Scale bar, 100 μm.
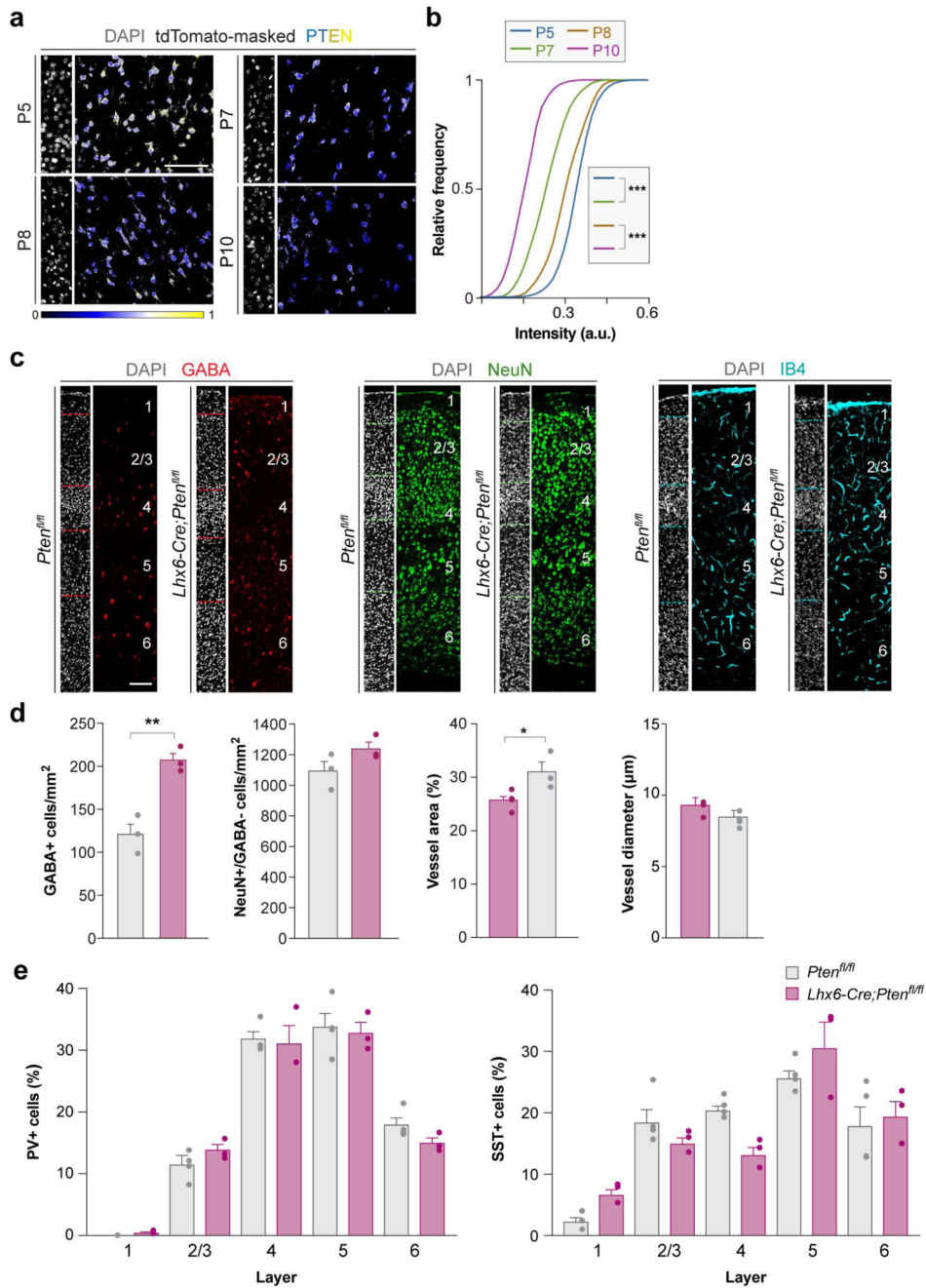
Extended Data Figure 8. PTEN expression in deep layer cortical interneurons and effects of loss of *Pten* function on neurons and blood vessels.
a, Coronal sections through layer 5 of S1BF from *Nkx2-1-Cre;RCL^tdTomato* mice at P5, P7, P8 and P10, immunostained PTEN and counterstained with DAPI (grey). PTEN expression is shown as a custom LUT in tdTomato-masked cells. **b**, Cumulative distribution of mean PTEN intensity in layer 5 and 6 MGE/POA interneurons (Kruskal-Wallis test, ***$p = 0$; $n =$ 7270 cells [P5], 4544 cells [P7], 6780 cells [P8] and 5043 cells [P10] from 3 different animals at each age). **c**, Coronal sections through S1BF from *Pten^fl/fl* and *Lhx6-Cre;Pten^fl/fl*

mice at P16 immunostained for GABA (red, left), NeuN (green, middle) and isolectin B4 (IB4, cyan, right) and counterstained with DAPI (grey). **d**, Quantification of the density of GABA (far left), NeuN+ but GABA- (left) cells, and vessel area (right) and diameter (far right) in P16 *Pten^{fl/fl}* (grey bars) and *Lhx6-Cre;Pten^{fl/fl}* (magenta bars) animals (2-tailed unpaired Student's *t*-test, **p = 0.0035 [GABA], *p = 0.0326 [vessel area], *p* = 0.0810 [vessel diameter]; Kolmogorov-Smirnov test, *p* = 0.1000 [NeuN+/GABA- cells], *n* = 3 animals for both genotypes). **e,** Quantification of the distribution of PV (left), SST (right) cells in P16 *Pten^{fl/fl}* (grey bars) and *Lhx6-Cre;Pten^{fl/fl}* (magenta bars) mice (2-way ANOVA, $F_{genotype}$ = 0.29, *p* = 0.61 [PV]; $F_{genotype}$ = 0.0004, *p* = 0.98 [SST]; *n* = 4 *Pten^{fl/fl}* animals and 3 *Lhx6-Cre;Pten^{fl/fl}* animals). Data is shown as mean ± SEM. Scale bars, 100 μm.
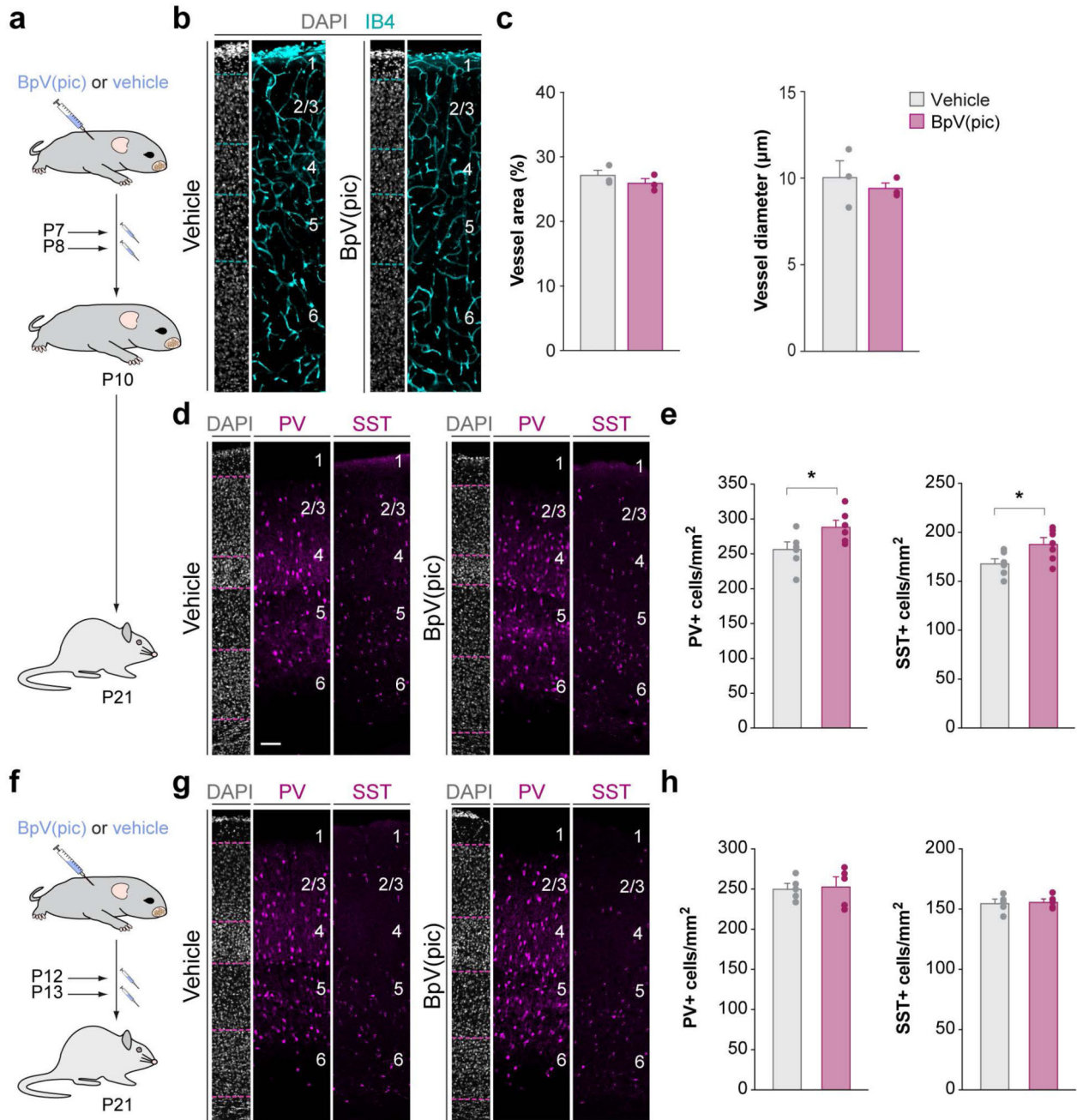
Extended Data Figure 9. Pharmacological PTEN inhibition during the interneuron cell death period increases interneuron survival.

a, **f**, Schematics of experimental design. **b,** Coronal sections through S1BF from P10 mice injected at P7-P8 with vehicle (left) or BpV(pic) (right) stained for isolectin B4 (IB4, cyan) and DAPI (grey). **c**, Quantification of blood vessel area (left) and diameter (right) in P10 mice treated with vehicle (grey bars) or BpV(pic) (magenta bars) (Kolmogorov-Smirnov test [vessel area], $p = 0.60$; 2-tailed unpaired Student's t-test [vessel diameter], $p = 0.58$, $n = 3$ animals for each group). **d**, **g**, Coronal sections through S1BF from P21 mice injected at P7-

P8 (**d**) or P12-P13 (**g**) with vehicle (left) or BpV(pic) (right) and immunostained for PV and SST and counterstained with DAPI. **e**, **h,** Quantification of the density of PV (left) and SST (right) in S1BF from P21 mice injected at P7-P8 (**e**) or P12-P13 (**h**) with vehicle (grey bars) or BpV(pic) (magenta bars) (P7-P8 groups: 2-tailed unpaired Student's t-test, *$p = 0.04$ [PV], *$p = 0.03$ [SST]; $n = 7$ animals for each group, P12-P13 groups: 2-tailed unpaired Student's t-test, $p = 0.84$ [PV], $p = 0.82$ [SST], $n = 5$ animals for each group). Data is shown as mean ± SEM. Scale bars, 100 μm.

Supplementary Material

Refer to Web version on PubMed Central for supplementary material.

Acknowledgements

References

1. Beaulieu C. Numerical data on neocortical neurons in adult rat, with special reference to the GABA population. Brain Res. 1993; 609:284–292. [PubMed: 8508310]

2. Meyer HS, et al. Inhibitory interneurons in a cortical column form hot zones of inhibition in layers 2 and 5A. Proc Natl Acad Sci USA. 2011; 108:16807–16812. [PubMed: 21949377]

3. Gabbott PL, Somogyi P. Quantitative distribution of GABA-immunoreactive neurons in the visual cortex (area 17) of the cat. Exp Brain Res. 1986; 61:323–331. [PubMed: 3005016]

4. Hendry SH, Schwark HD, Jones EG, Yan J. Numbers and proportions of GABA-immunoreactive neurons in different areas of monkey cerebral cortex. J Neurosci. 1987; 7:1503–1519. [PubMed: 3033170]

5. DeFelipe J, Alonso-Nanclares L, Arellano JI. Microstructure of the neocortex: comparative aspects. J Neurocytol. 2002; 31:299–316. [PubMed: 12815249]

6. Fishell G, Rudy B. Mechanisms of inhibition within the telencephalon: "where the wild things are". Annu Rev Neurosci. 2011; 34:535–567. [PubMed: 21469958]

7. Marín O. Interneuron dysfunction in psychiatric disorders. Nat Rev Neurosci. 2012; 13:107–120. [PubMed: 22251963]

8. Nelson SB, Valakh V. Excitatory/inhibitory balance and circuit homeostasis in autism spectrum disorders. Neuron. 2015; 87:684–698. [PubMed: 26291155]

9. Yizhar O, et al. Neocortical excitation/inhibition balance in information processing and social dysfunction. Nature. 2011; 477:171–178. [PubMed: 21796121]

10. Hamburger V, Levi-Montalcini R. Proliferation, differentiation and degeneration in the spinal ganglia of the chick embryo under normal and experimental conditions. J Exp Zool. 1949; 111:457–501. [PubMed: 18142378]

11. Yuan J, Yankner BA. Apoptosis in the nervous system. Nature. 2000; 407:802–809. [PubMed: 11048732]

12. Raff MC, et al. Programmed cell death and the control of cell survival: lessons from the nervous system. Science. 1993; 262:695–700. [PubMed: 8235590]

13. Green DR. Apoptotic pathways: the roads to ruin. Cell. 1998; 94:695–698. [PubMed: 9753316]

14. Southwell DG, et al. Intrinsically determined cell death of developing cortical interneurons. Nature. 2012; 491:109–113. [PubMed: 23041929]

15. Verney C, Takahashi T, Bhide PG, Nowakowski RS, Caviness VS Jr. Independent controls for neocortical neuron production and histogenetic cell death. Dev Neurosci. 2000; 22:125–138. [PubMed: 10657705]

16. Li Z, et al. Caspase-3 activation via mitochondria is required for long-term depression and AMPA receptor internalization. Cell. 2010; 141:859–871. [PubMed: 20510932]

17. Goebbels S, et al. Genetic targeting of principal neurons in neocortex and hippocampus of NEX-Cre mice. Genesis. 2006; 44:611–621. [PubMed: 17146780]

18. Xu Q, Tam M, Anderson SA. Fate mapping Nkx2.1-lineage cells in the mouse telencephalon. J Comp Neurol. 2008; 506:16–29. [PubMed: 17990269]

19. Price DJ, Aslam S, Tasker L, Gillies K. Fates of the earliest generated cells in the developing murine neocortex. J Comp Neurol. 1997; 377:414–422. [PubMed: 8989655]

20. Bartolini G, Ciceri G, Marín O. Integration of GABAergic interneurons into cortical cell assemblies: lessons from embryos and adults. Neuron. 2013; 79:849–864. [PubMed: 24012001]

21. Ikonomidou C, et al. Blockade of NMDA receptors and apoptotic neurodegeneration in the developing brain. Science. 1999; 283:70–74. [PubMed: 9872743]

22. Heck N, et al. Activity-dependent regulation of neuronal apoptosis in neonatal mouse cerebral cortex. Cereb Cortex. 2008; 18:1335–1349. [PubMed: 17965127]

23. Léveillé F, et al. Suppression of the intrinsic apoptosis pathway by synaptic activity. J Neurosci. 2010; 30:2623–2635. [PubMed: 20164347]

24. Madisen L, et al. Transgenic mice for intersectional targeting of neural sensors and effectors with high specificity and performance. Neuron. 2015; 85:942–958. [PubMed: 25741722]

25. Bortone D, Polleux F. KCC2 expression promotes the termination of cortical interneuron migration in a voltage-sensitive calcium-dependent manner. Neuron. 2009; 62:53–71. [PubMed: 19376067]

26. Priya R, et al. Activity regulates cell death within cortical interneurons through a Calcineurin-dependent mechanism. Cell Reports. 2018; 22:1695–1709. [PubMed: 29444424]

27. Denaxa M, et al. Modulation of apoptosis controls inhibitory interneuron number in the cortex. Cell Reports. 2018; 22:1710–1721. [PubMed: 29444425]

28. Anastasiades PG, et al. GABAergic interneurons form transient layer-specific circuits in early postnatal neocortex. Nat Commun. 2016; 7 10584.

29. Roth BL. DREADDs for Neuroscientists. Neuron. 2016; 89:683–694. [PubMed: 26889809]

30. Lindsten T, et al. The combined functions of proapoptotic Bcl-2 family members bak and bax are essential for normal development of multiple tissues. Mol Cell. 2000; 6:1389–1399. [PubMed: 11163212]

31. Dudek H, et al. Regulation of neuronal survival by the serine-threonine protein kinase Akt. Science. 1997; 275:661–665. [PubMed: 9005851]

32. Datta SR, et al. Akt phosphorylation of BAD couples survival signals to the cell-intrinsic death machinery. Cell. 1997; 91:231–241. [PubMed: 9346240]

33. Stambolic V, et al. Negative regulation of PKB/Akt-dependent cell survival by the tumor suppressor PTEN. Cell. 1998; 95:29–39. [PubMed: 9778245]

34. Backman SA, et al. Deletion of Pten in mouse brain causes seizures, ataxia and defects in soma size resembling Lhermitte-Duclos disease. Nat Genet. 2001; 29:396–403. [PubMed: 11726926]

35. Fogarty M, et al. Spatial genetic patterning of the embryonic neuroepithelium generates GABAergic interneuron diversity in the adult cortex. J Neurosci. 2007; 27:10935–10946. [PubMed: 17928435]

36. Lesche R, et al. Cre/loxP-mediated inactivation of the murine Pten tumor suppressor gene. Genesis. 2002; 32:148–149. [PubMed: 11857804]

37. Grigoriou M, Tucker AS, Sharpe PT, Pachnis V. Expression and regulation of Lhx6 and Lhx7, a novel subfamily of LIM homeodomain encoding genes, suggests a role in mammalian head development. Development. 1998; 125:2063–2074. [PubMed: 9570771]

38. Isaacson JS, Scanziani M. How inhibition shapes cortical activity. Neuron. 2011; 72:231–243. [PubMed: 22017986]

39. Xue M, Atallah BV, Scanziani M. Equalizing excitation-inhibition ratios across visual cortical neurons. Nature. 2014; 511:596–600. [PubMed: 25043046]

40. Burrone J, O'Byrne M, Murthy VN. Multiple forms of synaptic plasticity triggered by selective suppression of activity in individual neurons. Nature. 2002; 420:414–418. [PubMed: 12459783]

41. Maffei A, Nataraj K, Nelson SB, Turrigiano GG. Potentiation of cortical inhibition by visual deprivation. Nature. 2006; 443:81–84. [PubMed: 16929304]

42. Butt SJ, et al. The requirement of Nkx2-1 in the temporal specification of cortical interneuron subtypes. Neuron. 2008; 59:722–732. [PubMed: 18786356]

43. Cobos I, et al. Mice lacking Dlx1 show subtype-specific loss of interneurons, reduced inhibition and epilepsy. Nat Neurosci. 2005; 8:1059–1068. [PubMed: 16007083]

44. Glickstein SB, et al. Selective cortical interneuron and GABA deficits in cyclin D2-null mice. Development. 2007; 134:4083–4093. [PubMed: 17965053]

45. Lui JH, Hansen DV, Kriegstein AR. Development and evolution of the human neocortex. Cell. 2011; 146:18–36. [PubMed: 21729779]

46. Florio M, Huttner WB. Neural progenitors, neurogenesis and the evolution of the neocortex. Development. 2014; 141:2182–2194. [PubMed: 24866113]

47. Butler MG, et al. Subset of individuals with autism spectrum disorders and extreme macrocephaly associated with germline PTEN tumour suppressor gene mutations. J Med Genet. 2005; 42:318–321. [PubMed: 15805158]

48. Buxbaum JD, et al. Mutation screening of the PTEN gene in patients with autism spectrum disorders and macrocephaly. Am J Med Genet B Neuropsychiatr Genet. 2007; 144B:484–491. [PubMed: 17427195]

49. Blanquie O, et al. Electrical activity controls area-specific expression of neuronal apoptosis in the developing mouse cerebral cortex. Elife. 2017; 6

50. DeFelipe J. Types of neurons, synaptic connections and chemical characteristics of cells immunoreactive for calbindin-D28K, parvalbumin and calretinin in the neocortex. J Chem Neuroanat. 1997; 14:1–19. [PubMed: 9498163]

51. Mort RL, et al. Fucci2a: a bicistronic cell cycle reporter that allows Cre mediated tissue specific expression in mice. Cell Cycle. 2014; 13:2681–2696. [PubMed: 25486356]

52. Fazzari P, et al. Control of cortical GABA circuitry development by Nrg1 and ErbB4 signalling. Nature. 2010; 464:1376–1380. [PubMed: 20393464]

53. West MJ, Gundersen HJ. Unbiased stereological estimation of the number of neurons in the human hippocampus. J Comp Neurol. 1990; 296:1–22. [PubMed: 2358525]

54. Chen TW, et al. Ultrasensitive fluorescent proteins for imaging neuronal activity. Nature. 2013; 499:295–300. [PubMed: 23868258]

55. Green DM, Swets JA. Signal detection theory and psychophysics. Wiley; 1966.

56. Krashes MJ, et al. Rapid, reversible activation of AgRP neurons drives feeding behavior in mice. J Clin Invest. 2011; 121:1424–1428. [PubMed: 21364278]

57. Laemmli UK. Cleavage of structural proteins during the assembly of the head of bacteriophage T4. Nature. 1970; 227:680–685. [PubMed: 5432063]

58. Carpenter AE, et al. CellProfiler: image analysis software for identifying and quantifying cell phenotypes. Genome Biol. 2006; 7:R100. [PubMed: 17076895]
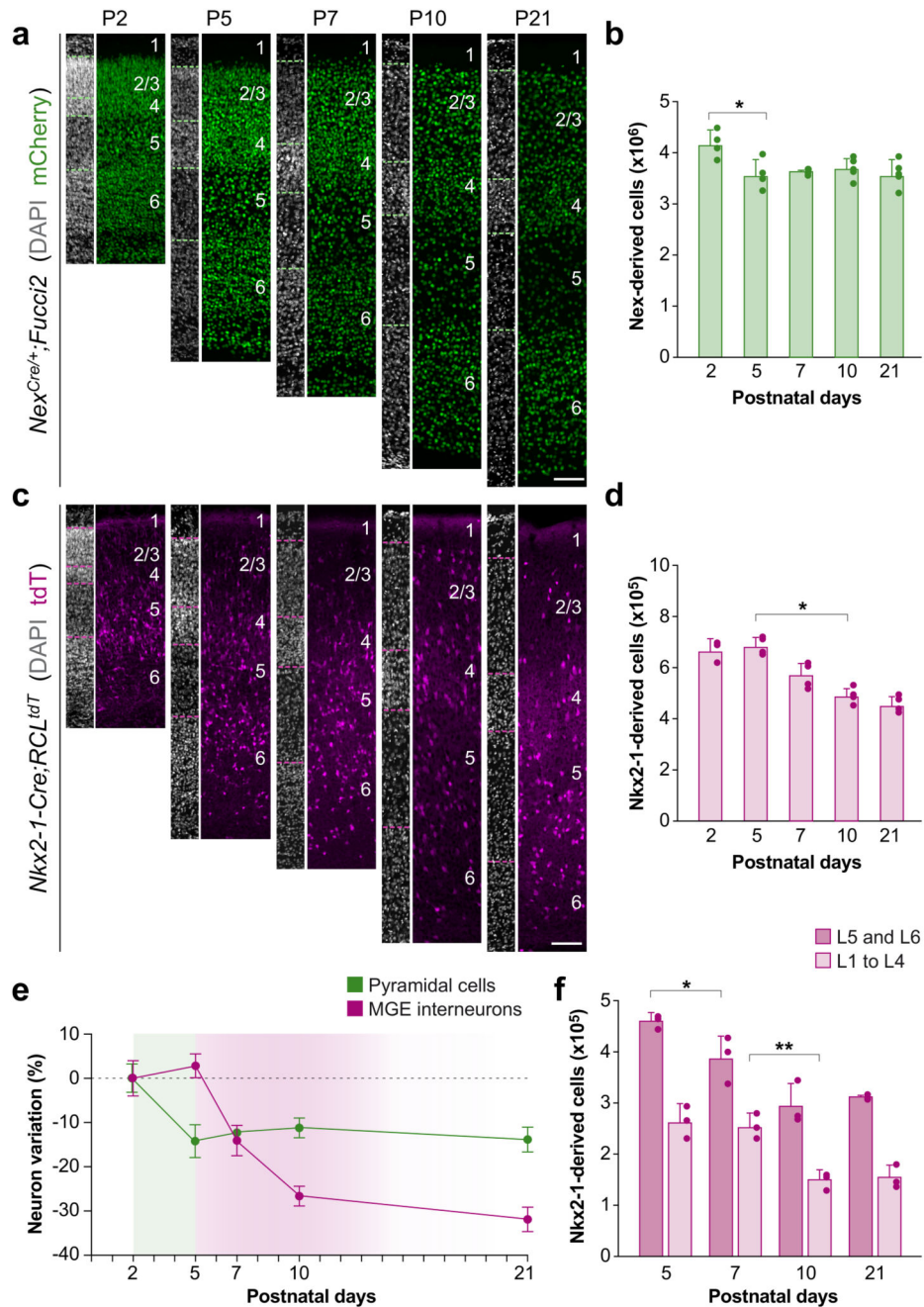
Figure 1. Consecutive waves of programmed cell death for pyramidal cells and interneurons in the early postnatal cortex.

a, **c**, Coronal sections through the primary somatosensory cortex (S1) of *Nex^Cre;Fucci2* (**a**) and *Nkx2-1-Cre;RCL^tdTomato* (**c**) mice during postnatal development. **b,** Total number of pyramidal cells in the entire neocortex of *Nex^Cre;Fucci2* mice (ANOVA, F = 4.17, *p = 0.02; n = 4 [P2 and P5], 3 [P7] and 5 [P10 and P21] animals). **d,** Total number of MGE/POA interneurons in the entire neocortex of *Nkx2-1-Cre;RCL^tdTomato* mice (ANOVA, F = 26.80, *p = 0.01; n = 4 animals for all ages). **e**, Temporal variation in pyramidal cell and

MGE/POA interneuron percentages. **f**, Total number of MGE/POA interneurons in superficial (L1-L4) and deep layers (L5 and L6) of the neocortex (2-way ANOVA, $F_{interaction}$ = 1.01,*p = 0.03 and **p = 0.002; n = 3 animals for all ages). Data is shown as mean ± SEM. Scale bars, 100 μm.
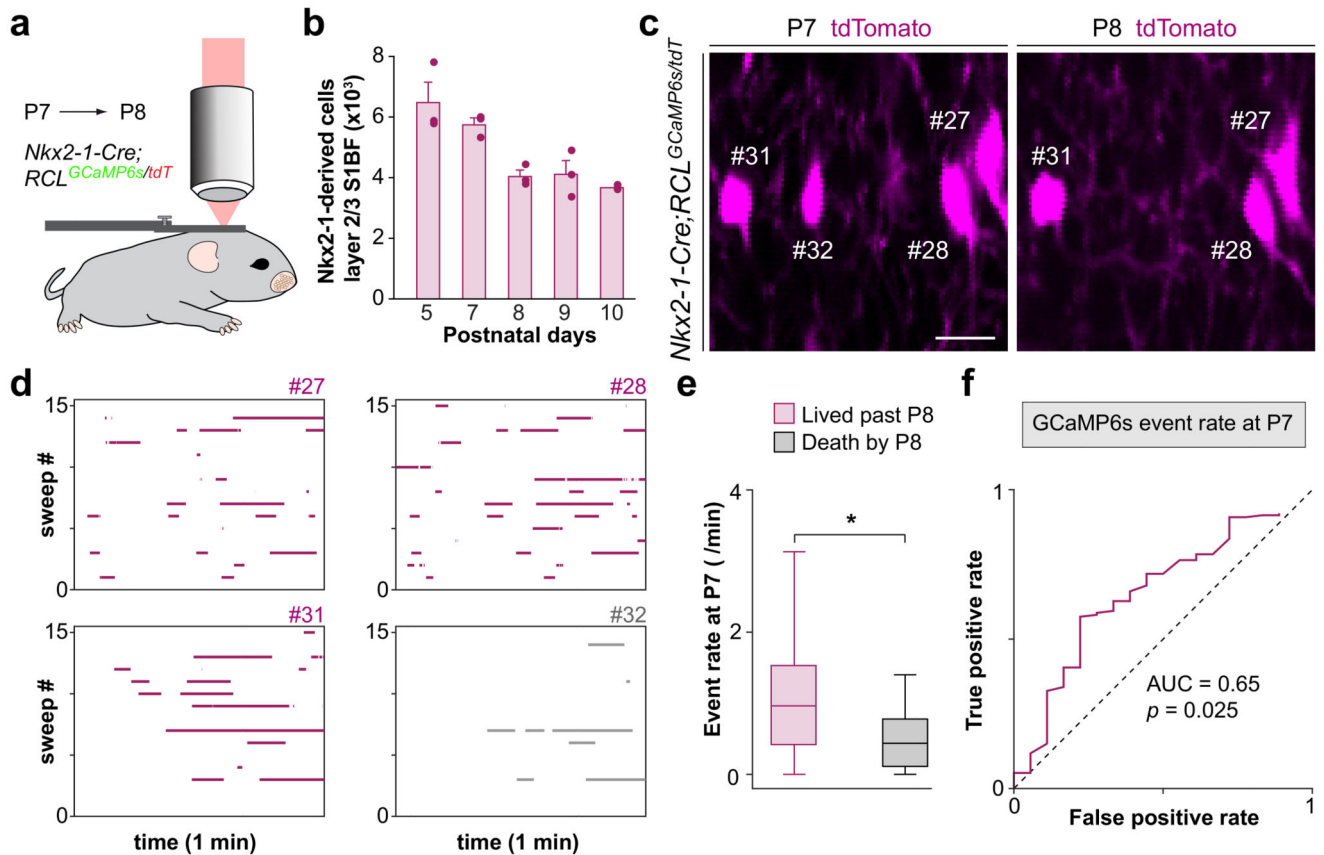
Figure 2. Interneuron activity levels predict cell death.
a, Schematic of experimental design. **b,** Total number of MGE/POA interneurons in layer 2/3 S1BF of *Nkx2-1-Cre;RCL*^tdTomato^ mice (*n* = 3 animals for all ages). Data is shown as mean ± SEM. **c,** ROI imaged at P7 (left) and P8 (right). **d**, Raster plots showing the occurrence of calcium events at P7 for the four neurons shown in (**c**). **e**, Box plots illustrating event rates for P7 interneurons that live past P8 (magenta) and interneurons that die by P8. Two-sided Mann-Whitney test, *p* = 0.03; *n* = 18 for cells that die at P8 and 153 for cells that live beyond P8, from 3 different pups. **f**, ROC analysis showing the ability of P7 event rates to discriminate between cells that die by P8 and cells that live past P8, AUC (area under the curve) = 0.65, *p* = 0.025. Scale bar, 15 μm.
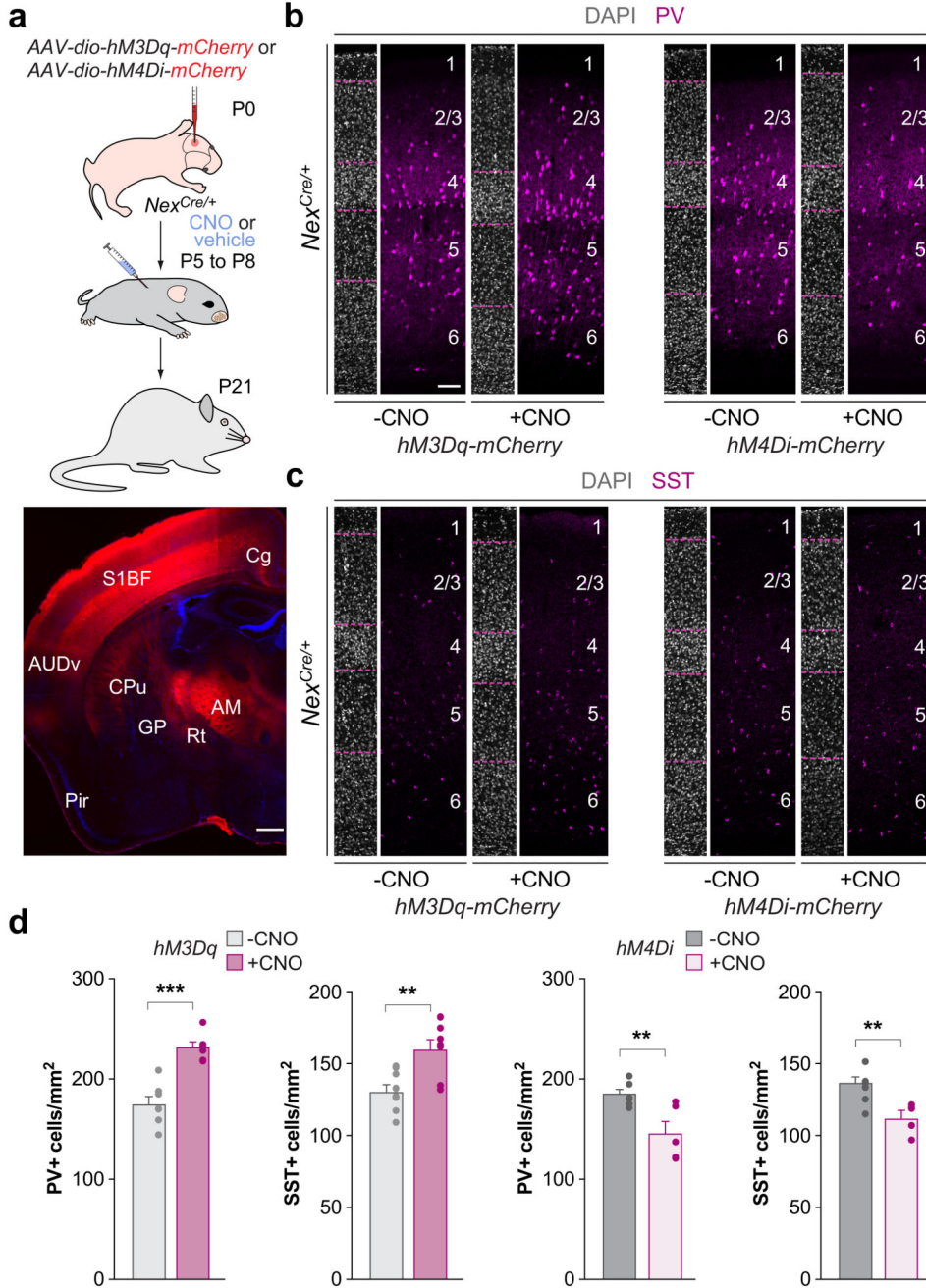
Figure 3. Bidirectional modulation of pyramidal cell activity regulates the extent of interneuron cell death.

a, Schematic of experimental design. mCherry expression at P21 following AAV injection at P0. **b**, **c**, Coronal sections through S1BF from P21 *Nex^Cre/+* mice injected with *hM3Dq-mCherry* or *hM4Di-mCherry* viruses followed by vehicle or CNO treatment. **d**, Quantification of the density of PV and SST cells at P21. Two-tailed Student's unpaired *t*-test, for hM3DQ, ***$p = 0.0002$, **$p = 0.003$; for hM4DI, **$p = 0.006$ [PV], **$p = 0.004$ [SST]; for hM3DQ, $n = 7$ and 9 animals for -CNO PV and SST, respectively; 6 and 7

animals for +CNO PV and SST, respectively; for hM4DI, $n = 7$ animals for -CNO and 5 animals for +CNO for both PV and SST. Data is shown as mean ± SEM. Scale bars, 500 μm (**a**) and 100 μm (**b**).
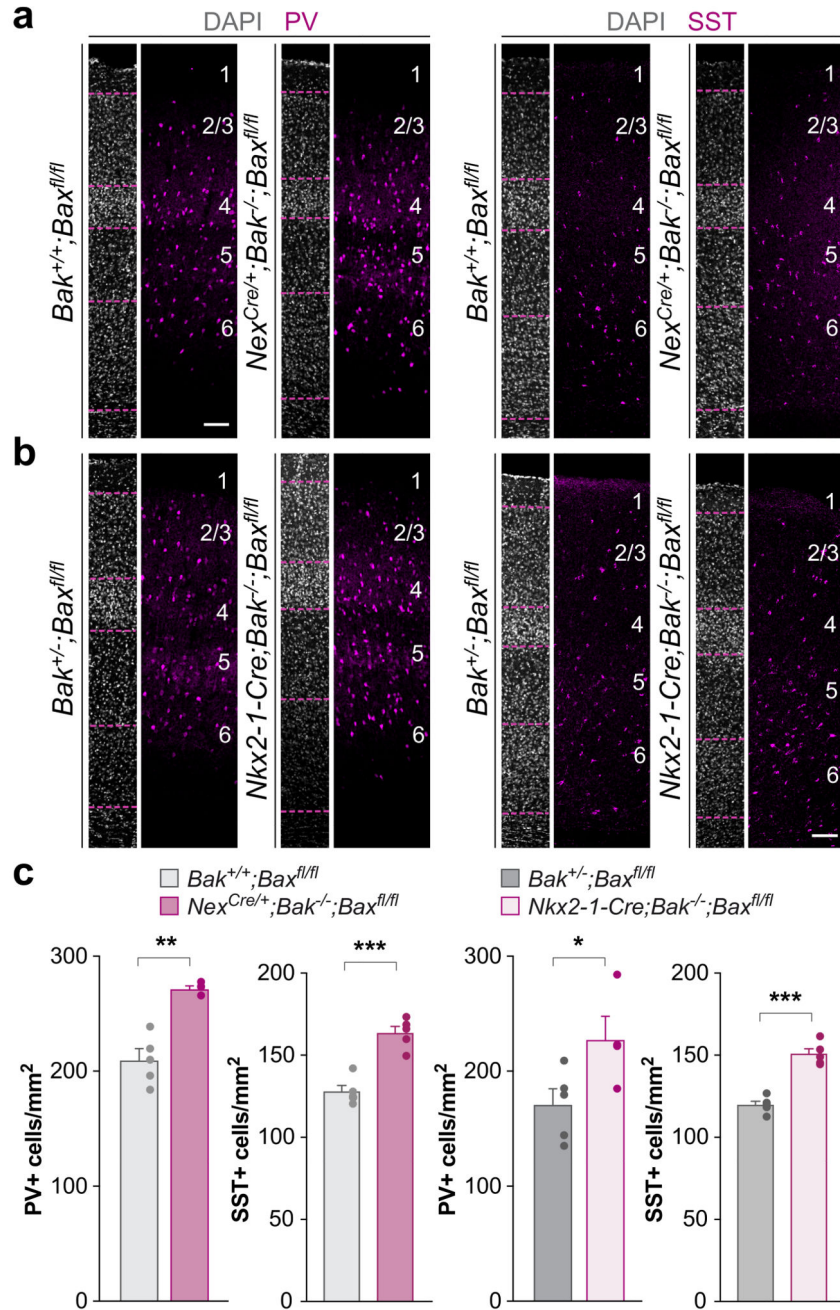
Figure 4. Survival of pyramidal cells rescues interneuron cell death.
a, **b**, Coronal sections through S1BF from P30 $Bak^{+/+};Bax^{fl/fl}$ and $Nex^{Cre/+};Bak^{-/-};Bax^{fl/fl}$
(**a**), and $Bak^{+/-};Bax^{fl/fl}$ and $Nkx2\text{-}1\text{-}Cre;Bak^{-/-};Bax^{fl/fl}$ (**b**) mice. **c**, Quantification of the
density of PV and SST cells in pyramidal cell-specific Bax/Bak mutant mice, MGE/POA
interneuron-specific Bax/Bak mutant mice and their respective controls at P30. Two-tailed
Student's unpaired t-test, for $Nex^{Cre/+}$, $**p = 0.001$, $***p = 0.0002$; for $Nkx\text{-}2\text{-}1\text{-}Cre$, $*p = 0.04$, $***p = 0.00004$; $n = 4$ animals for $Nex^{Cre/+};Bak^{-/-};Bax^{fl/fl}$ [PV] and 5 animals for all
other groups. Data is shown as mean $\pm$ SEM. Scale bar, 100 μm.
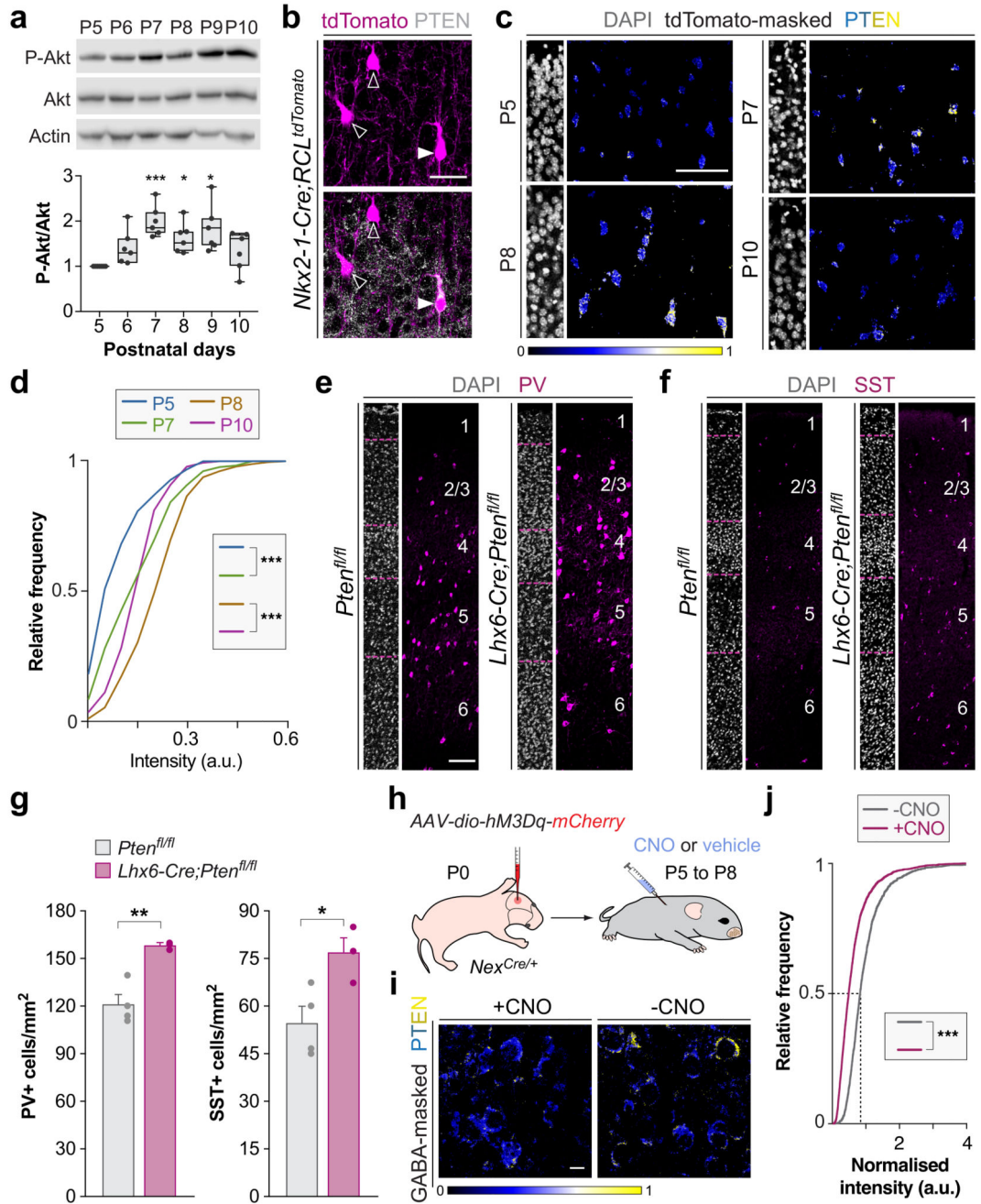
Figure 5. Pyramidal cell activity controls interneuron cell survival through PTEN inhibition.
a, P-Akt, Akt and Actin protein levels in the neocortex. Friedman test, $p = 0.001$; *$p = 0.03$ for P5 vs P8, *$p = 0.0101$ for P5 vs P9 and ***$p = 0$ for P5 vs P7; $n = 6$ animals for all ages. **b**, Coronal section through layer 2/3 S1BF from *Nkx2-1-Cre;RCL*[tdTomato] mice at P8. Some interneurons have much higher PTEN levels (arrowhead) than most (open arrowheads). **c**, Coronal sections through layer 2/3 S1BF from *Nkx2-1-Cre;RCL*[tdTomato] mice at P5, P7, P8 and P10. PTEN expression is shown as a custom LUT in tdTomato-masked cells. **d**, Cumulative distribution of mean PTEN intensity in layer 2/3 MGE interneurons. Kruskal-

Wallis, ***$p = 1.7 \times 10^{-54}$; $n = 223$ cells [P5], 184 cells [P7], 394 cells [P8] and 395 cells [P10] from 3 different animals at each age. **e, f,** Coronal sections through S1BF from *Pten^{fl/fl}* and *Lhx6-Cre;Pten^{fl/fl}* mice at P16. **g,** Quantification of the density of PV and SST cells in P16 *Pten^{fl/fl}* and *Lhx6-Cre;Pten^{fl/fl}* mice. Two-tailed Student's *t*-test, *$p = 0.04$, **$p = 0.005$; $n = 4$ *Pten^{fl/fl}* and 3 *Lhx6-Cre;Pten^{fl/fl}* animals. **h,** Schematic of experimental paradigm. **i,** Coronal sections through layer 2/3 S1BF from P8 *Nex^{Cre/+}* mice injected with hM3Dq-mCherry at P0 followed by vehicle or CNO treatment. PTEN expression is shown as a custom LUT in GABA-masked cells. **j,** Normalised cumulative distribution of PTEN intensity in layer 2/3 S1BF GABAergic cells in vehicle and CNO-treated mice. Kolmogorov-Smirnov test, *** $p = 1.05 \times 10^{-111}$; $n = 1191$ cells [vehicle] and 3231 cells [CNO] from 4 vehicle and 8 CNO-treated animals. Data is shown as mean ± SEM. Scale bars, 50 μm (**b**), 100 μm (**c, e, f**), and 10 μm (**j**).